Shapeable magnetoelectronics

Denys Makarov, Michael Melzer, Daniil Karnaushenko, et al.

View Online   Export Citation   CrossMark

ARTICLES YOU MAY BE INTERESTED IN

APPLIED PHYSICS REVIEWS—FOCUSED REVIEW

Shapeable magnetoelectronics

Denys Makarov,[1,2,a)] Michael Melzer,[1,a)] Daniil Karnaushenko,[1] and Oliver G. Schmidt[1]

[1]*Institute for Integrative Nanosciences, Leibniz Institute for Solid State and Materials Research Dresden (IFW Dresden), Helmholtzstr. 20, 01069 Dresden, Germany*
[2]*Helmholtz-Zentrum Dresden-Rossendorf e.V., Institute of Ion Beam Physics and Materials Research, 01328 Dresden, Germany*

Inorganic nanomembranes are shapeable (flexible, printable, and even stretchable) and transferrable to virtually any substrate. These properties build the core concept for new technologies, which transform otherwise rigid high-speed devices into their shapeable counterparts. This research is motivated by the eagerness of consumer electronics towards being thin, light-weight, flexible, and even wearable. The realization of this concept requires all building blocks as we know them from rigid electronics (e.g., active elements, optoelectronics, magnetoelectronics, and energy storage) to be replicated in the form of (multi)functional nanomembranes, which can be reshaped on demand after fabrication. There are already a variety of shapeable devices commercially available, i.e., electronic displays, energy storage elements, and integrated circuitry, to name a few. From the beginning, the main focus was on the fabrication of shapeable high-speed electronics and optoelectronics. Only very recently, a new member featuring magnetic functionalities was added to the family of shapeable electronics. With their unique mechanical properties, the shapeable magnetic field sensor elements readily conform to ubiquitous objects of arbitrary shapes including the human skin. This feature leads electronic skin systems beyond imitating the characteristics of its natural archetype and extends their cognition to static and dynamic magnetic fields that by no means can be perceived by human beings naturally. Various application fields of shapeable magnetoelectronics are proposed. The developed sensor platform can equip soft electronic systems with navigation, orientation, motion tracking, and touchless control capabilities. A variety of novel technologies, such as smart textiles, soft robotics and actuators, active medical implants, and soft consumer electronics, will benefit from these new magnetic functionalities. This review reflects the establishment of shapeable magnetic sensorics, describing the entire development from the first attempts to verify the functional concept to the realization of ready-to-use highly compliant and strain invariant sensor devices with remarkable robustness. *© 2016 Author(s). All article content, except where otherwise noted, is licensed under a Creative Commons Attribution (CC BY) license (http://creativecommons.org/licenses/by/4.0/).* [http://dx.doi.org/10.1063/1.4938497]

TABLE OF CONTENTS

a)Authors to whom correspondence should be addressed. Electronic addresses: d.makarov@hzdr.de and m.melzer@ifw-dresden.de

I. INTRODUCTION

Electronics of tomorrow will be compliant and will form a seamless link between soft or even living materials and the digital world. For this purpose, electronic systems have to become flexible or even attain the possibility to reversibly accommodate tensile strains far beyond the intrinsic ductility of the active electronic materials they are made of. Shapeable, namely, flexible,[1–3] printable,[4] and stretchable,[5–7] electronics became one of the most vital technological research fields of the latest years, aiming to revolutionize common electronic systems towards being arbitrarily reshapeable on demand after their fabrication, particularly on large areas using cost-efficient printing technologies.

Organic electronic materials have been extensively used to create shapeable systems with various functionalities[8–10] even featuring active matrix addressing capabilities.[11,12] Compliant designs of inorganic semiconductor[5,13,14,192] and metal-based[15–18] electronics, however, combine the advantages of being soft with the high speed and low power consumption capabilities of conventional semiconductor-based electronics.[19] A large variety of compliant organic and inorganic electronic elements with various functions have been realized in the last years (Figure 1), including light emitting diodes (LEDs),[20,21] heaters,[12] actuators,[22] and supercapacitors.[23] Shapeable sensory devices can detect mechanical,[18,24–26] optical,[27] thermal,[28,29] or bioelectric[30,31] stimuli. The powering of prospective soft electronics may be assured by incorporated stretchable solar cells,[9,32] energy harvesters,[33–35] or batteries,[36,37] or even wirelessly.[15,38] Recent developments aim to add further useful features beyond shapeability: Transient electronics[39,40] is able to completely dissolve upon fulfilling its task after a defined period of time and imperceptible forms of electronic systems[12,29,41] are haptically not perceived if worn on skin.

One of the prominent development directions is the field of *electronic skins* (e-skins),[38,44–46] which are conformably situated on biological tissue, readily following all its natural motions and distortions (Figure 2). In addition to being wearable, e-skins can also be operated *in vivo* as bio-integrated electronics,[47–50] enabling highly functional and compliant diagnostic or therapeutic implants[31] as well as advanced surgical tools.[51] Stretchability of functional electronic elements is also expected to have high potential for wearable devices[35,52] and smart textiles.[53,54] Another novel field of prospective applications for shapeable electronics is *soft*
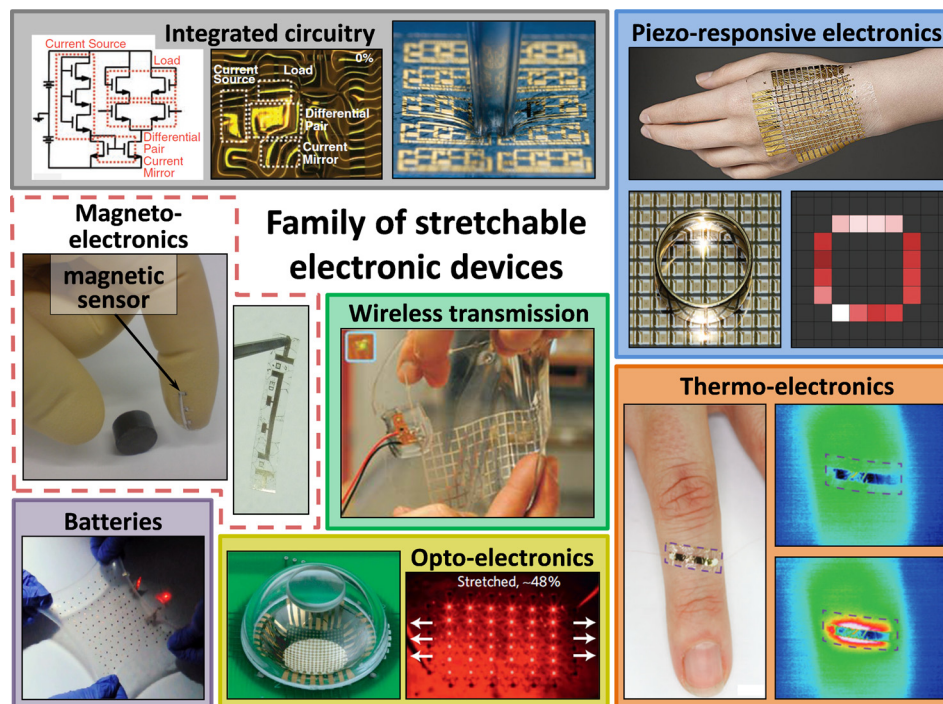
FIG. 1. Overview of available functionalities in stretchable electronic devices: Various capabilities have been demonstrated already. Stretchable magnetoelectronics, which is introduced in this work, adds magnetic functionalities and is also included as a new member in this family. Reprinted with permission from Kim *et al.*, Science **320**, 507 (2008). Copyright 2008 AAAS; Reprinted with permission from Rogers *et al.*, Science **327**, 1603 (2010). Copyright 2010 AAAS; Reprinted with permission from Kaltenbrunner *et al.*, Nature **499**, 458 (2013). Copyright 2013 Macmillan Publishers Ltd.; Reprinted with permission from Kim *et al.*, Nat. Mater. **9**, 929 (2010). Copyright 2010 Macmillan Publishers Ltd.; Reprinted with permission from Ko *et al.*, Nature **454**, 748 (2008). Copyright 2008 Macmillan Publishers Ltd.; Reprinted with permission from Xu *et al.*, Nat. Commun. **4**, 1543 (2013). Copyright 2013 Macmillan Publishers Ltd.; Reproduced with permission from Cheng *et al.*, Lab Chip **10**, 3227 (2010). Copyright 2010 The Royal Society of Chemistry; Reproduced with permission from Melzer *et al.*, Nano Lett. **11**, 2522 (2011). Copyright 2011 American Chemical Society.

Electronic skins   **Functional implants**   **Soft robotics**   **Smart textiles**

FIG. 2. Application fields of stretchable electronics: Overview of applications for soft electronics with prospective potential for stretchable magnetic sensorics. Reprinted with permission from Kim *et al.*, Nat. Mater. **10**, 316 (2011). Copyright 2011 Macmillan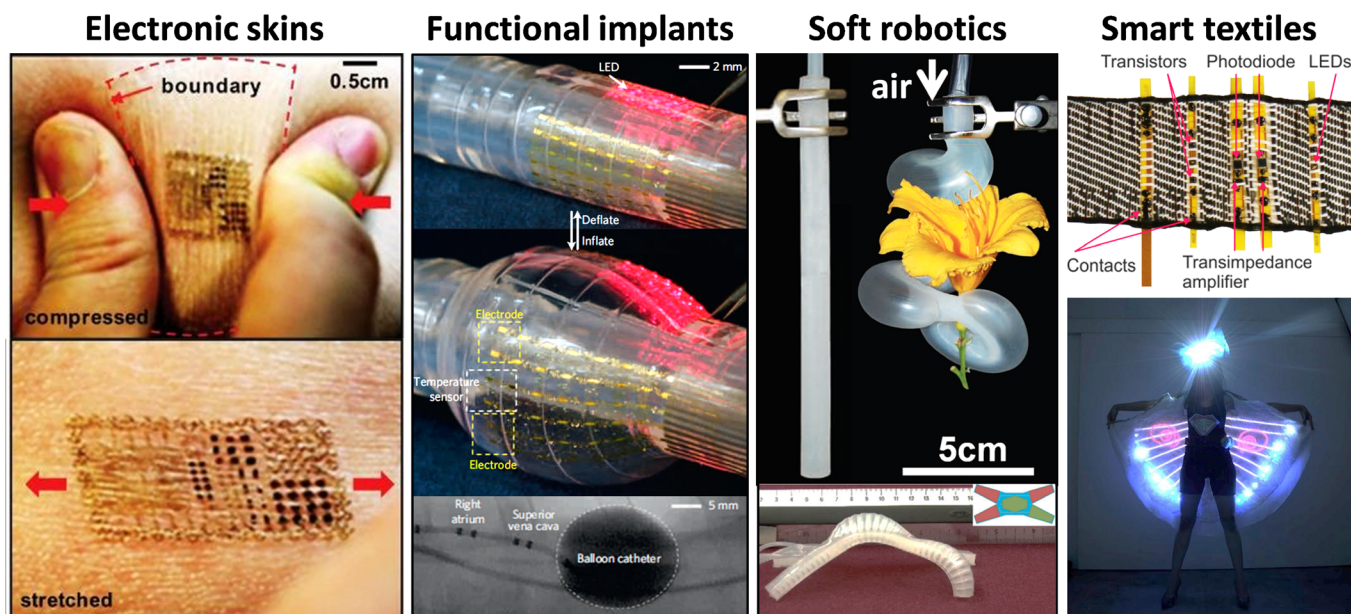 Publishers Ltd.; Reprinted with permission from Kim *et al.*, Science **333**, 838 (2011). Copyright 2011 AAAS; Reprinted with permission from Martinez *et al.*, Adv. Mater. **25**, 205 (2013). Copyright 2013 John Wiley & Sons, Inc.; Reproduced with permission from Shepherd *et al.*, Proc. Natl. Acad. Sci. U. S. A. **108**, 20400 (2011). Copyright 2011 The National Academy of Sciences of the U.S.A.; Reproduced with permission from Zysset *et al.*, Opt. Express **21**, 3213 (2013). Copyright 2013 Optical Society of America;[65] and Adapted from http://smarttextiles.se.[66]

robotics,[55,56] particularly *elastomeric actuators*.[22,57] This novel actuator technology allows for a lightweight,[58] indestructible,[59] and adaptive[60] design of robotics that may even feature cloaking capabilities.[61] Their large actuation strains[22,62] and rapid motion[63,64] call for an extraordinary compliant form of electronics to be integrated into this kind of electromechanical transducers.

A. Magnetic functionalities for shapeable electronics

Despite the manifold functionalities that are available for shapeable electronic systems, magnetic functionality (Figure 1) was added to the family of flexible,[67–73] printable,[74–76] stretchable,[43,77,78] and even imperceptible[79] electronics very recently.

Since the acquisition of motion and displacement has been developed to be the main duty of magnetic sensorics in conventional machinery, a shapeable counterpart can adopt these functions into soft systems. Hence, as electronic skin, magnetic sensing elements would be ideally suited for touchless human-machine interaction, by means of accurate motion tracking in an artificial magnetic environment.[79] In the field of bio-integrated electronics and functional implants, magnetic sensing capabilities could include real time monitoring of muscles, joints, or valves of the heart to diagnose early stages of dysfunctions. The displacement sensing capabilities can also play a key role for the recording and accurate control of actuation in soft robotic systems.[55,56] As for their rigid counterparts, keeping track of the current position of all its movable parts is an essential requirement for highly functional robots with multi-tasking abilities. This is even more vital to soft robots, as the displacement of actuating components is strongly dependent on the mechanical load on these parts. Control strategies relying on the feedback from magnetic motion tracking sensorics can provide a comprehensive, highly integrative, and cost effective solution to this issue compared to, e.g., optical approaches. Foreseeable applications of highly sensitive and re-shapeable magnetoelectronics also include the in-flow detection of magnetic particles or magnetically labeled analytes,[70,80] in advanced fluidics[81] and lab-on-a-chip[82] platforms, which may boost the health monitoring, point-of-care diagnostics, and environmental sensing capabilities of these systems. Furthermore, shapeable forms of consumer electronics[83] and smart textiles[53,54] will benefit from magnetic functionalities offered by compliant magnetoelectronics.

The commercialization potential of flexible electronics is greatly enhanced by the use of large-area cost-efficient printing technologies, providing identification tags to track goods in shops and large area displays for television sets (TVs) and smartphones, to name just a few. The grand vision behind this smart combination of large-area printable and flexible electronics is towards commercializing *intelligent* packaging, postcards, or promotional materials that communicate with the environment and provide a response to the customer, in the spirit of the Internet of Things (IoT) technology. The realization of this vision relies on the availability of printable electronic components that are *energy efficient*, to extend the autonomous lifetime of the devices. The most energy efficient electronic components are electromagnetic switches based on magnetoresistive elements. Their operation current is less than 1 mA, and they work in conjunction with permanent magnets which do not need a power supply. These high-performance printable magnetic switches are, although highly demanded, not available on the market, yet.

In this review, we cover both fundamental and application relevant aspects of the emergent field of shapeable

magnetoelectronics. The article is organized as follows: The following three sections introduce topic-wise flexible (Sec. II), printable (Sec. III), and stretchable (Sec. IV) magnetic sensorics. This information is crucial to follow the development, which led to the very recent realization of imperceptible magnetoelectronics (Sec. V). To facilitate reading, the technological relevance as well as the future development directions of each branch of shapeable magnetosensorics is given directly in the respective sections. The article is briefly summarized in Sec. VI by providing an outlook for the prospective applications.

II. FLEXIBLE MAGNETIC SENSOR DEVICES

Depending on the desired properties (i.e., sensitivity, magnetic field range, sensitive direction, and temperature behavior), there are several technologies available for the realization of magnetic sensing devices.[84] These include, for example, Hall sensors,[85] magnetoresistance and anisotropic magnetoresistance elements,[86] magnetic tunnel junctions,[87] magnetoimpedance,[88–91] as well as fluxgate magnetometers.[92] Some of these sensorics, including Hall effect, magnetoresistive, and magnetoimpedance devices, are already realized in the flexible form.

A. Hall effect sensorics

Next generation flexible appliances aim to become fully autonomous and will require ultra-thin and flexible navigation modules, body tracking, and relative position monitoring systems. Key building blocks of navigation and position tracking devices are Hall effect sensors. Conventional semiconductor-based Hall sensors are about 400-μm thick and rigid, limiting their direct applicability in flexible electronics. To overcome this limitation of the conventional technology, a novel technology platform was introduced relying on the smart combination of functional inorganic nanomembranes and polymeric foils that allowed to fabricate *entirely flexible* Hall effect sensorics (Figure 3).[71,93,94] This is achieved by combining inorganic Bismuth

nanomembranes with polymeric Polyimide (PI) or Polyether Ether Ketone (PEEK) foils.

The advantages of using bismuth for Hall probes are mainly the cost effective preparation and structuring by standard thin film deposition and lithographic methods.[95] This is, in particular, important for thin and flexible sensors, as metal films can be deposited on various substrates, including polymers and plastic foils. Furthermore, due to its negligible surface charge depletion effects,[96] Bi Hall probes show significant signal-to-noise ratio at room temperature even at sub-μm lateral sizes, which is not the case for conventional semiconductor-based Hall effect sensors.

By thorough thickness optimization of the inorganic Bi film and a temperature treatment procedure, the entirely flexible Hall effect sensorics is realized with a near bulk sensitivity of -2.3 V/AT (Figure 3(h)). This outstanding performance of the flexible devices is achieved due to the careful tailoring of the morphology of the thin Bismuth films grown on flexible foils. The flexible sensors withstand severe mechanical deformations with only a minor reduction in sensor performance, as observed when bent into a radius of 6 mm, which is fully recovered in the flat state.

1. Technological relevance

The technological relevance of the proposed fabrication approach was demonstrated by preparing the flexible Bismuth Hall sensors onto commercial flexible printed circuit (FPCs) boards. In addition to single sensors providing a point-like measurement of the magnetic flux density (Figures 3(a), 3(f), and 3(g)), 1D linear sensor arrays are also prepared on FPCs (Figures 3(d) and 3(e)), which defines the Hall-cross contact geometries and sensor arrangements.[71] For demonstration purposes, these sensor arrays were applied to reconstruct a spatial and temporal profile of a varying magnetic field. In order to reduce disturbances from Eddy currents during operation of the prepared sensors for high frequency applications, as typical for, e.g., actively controlled magnetic bearings, loops in the conducting parts have to be avoided. By using twisted wires, the flexible Hall sensorics were efficiently applied to realize flux based

Flexible Hall sensors for wearable electronics

Flexible Hall sensors on FPCs for eMobility applications

Optimized sensor with near bulk performance
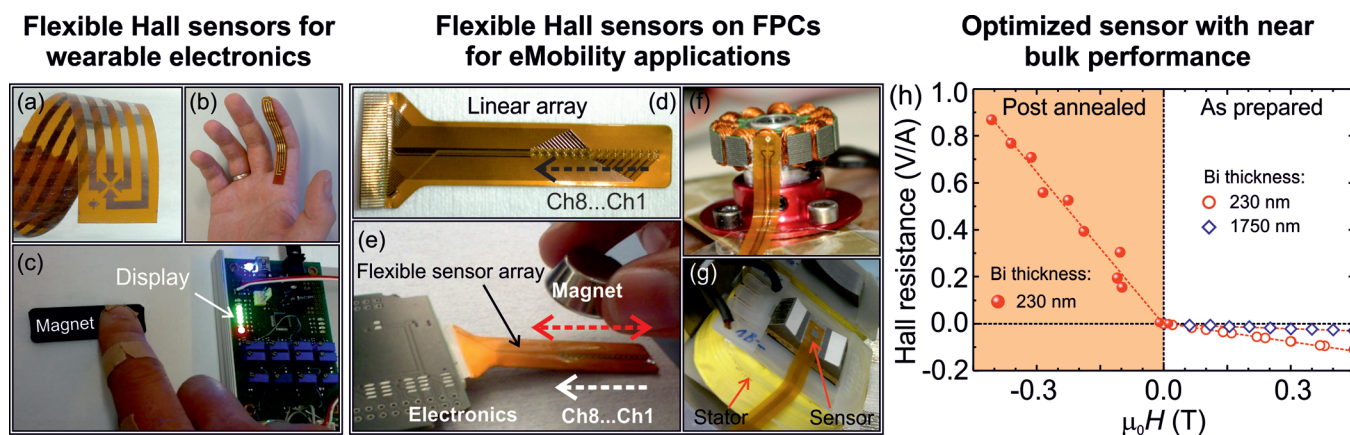
FIG. 3. Entirely flexible Hall effect sensorics (a), which can be used as a functional element for wearable electronics (b) and (c). The approach can be extended to fabricate Hall sensors on commercial flexible printed circuit boards, FPCs (d) and (e), for monitoring electrical motors (f) or magnetic bearing systems (g). After optimization, the flexible sensors reveal near bulk sensitivity (h). Reprinted with permission from Melzer *et al.*, Adv. Mater. **27**, 1274 (2015). Copyright 2015 John Wiley & Sons, Inc.

control scheme for magnetic levitation,[97] where the measured air gap flux density is used as controller feedback for magnetically suspended systems.[94]

Applications of the proposed technology platform are far-reaching: The sensor can be bent around the wrist or positioned on the finger to realize an interactive pointing device that visualizes the relative position of the finger with respect to a magnetic field, thus creating a unique feedback element for wearable electronics (Figures 3(b) and 3(c)). Apart from flexible and wearable consumer electronics, thin and bendable Hall sensors are of great interest for integration into electrical machines and drives, allowing for the optimization of eMotor designs and performance of magnetic bearing systems (Figures 3(f) and 3(g)). Featuring a flat and flexible design, they can be positioned inside the typically curved and narrow ($<500\,\mu m$) air gaps between rotor and stator in order to provide a direct magnetic field measurement, which is not feasible with current chip-based rigid sensing elements.

B. Magnetoresistive sensing devices

In contrast to Hall effect sensorics, which can be applied also for large magnetic field measurements in the Tesla range, high performance magnetic field sensorics relying on giant magnetoresistance (GMR) or tunneling magnetoresistive (TMR) effect can be efficiently used as on-off sensors for magnetic switch applications or for measurement of small magnetic fields in the range of mT or below. Magnetic thin films revealing a GMR effect are able to vary their electrical resistance by several tens of percent upon application of an external magnetic field.[98] The utilization of GMR- and TMR-based sensorics, for example, in magnetic read heads[99] boosted the capacity and performance of magnetic data storage systems. Currently, GMR sensor devices are fabricated on rigid inorganic substrates like oxidized silicon (SiOx) wafers or glass. Exemplary response curves measured on standard GMR stacks of Co/Cu and Py/Cu multilayers ($Py = Fe_{81}Ni_{19}$ alloy) are shown in Figure 4. The GMR ratio is obtained by the change of electrical resistance $R(H)$ relative to the value at magnetic saturation R_{sat}

$$GMR = 100\% \cdot \frac{R(H) - R_{sat}}{R_{sat}} \qquad (2.1)$$

and is usually expressed in percent.[100] The field dependent sensitivity $S(H)$ of a magnetoresistive element, which is defined as the first derivative of the sample's resistance over the magnetic field divided by the resistance value[100]

$$S(H) = \left[\frac{dR(H)}{dH}\right] \Big/ R(H) \qquad (2.2)$$

is also provided in the graphs.

The sensitivity of GMR multilayers can be enhanced by using soft magnetic materials, e.g., Py instead of Co and by going from the first to the 2nd antiferromagnetic coupling maximum[98] (compare panels (a) and (b) in Figure 4). The weaker coupling strength between the FM layers results is a magnetization alignment at much lower fields. Although the GMR magnitude is reduced in this case and also magnetic saturation occurs at much lower fields, the sensitivity in this regime is increased significantly rendering them appropriate as sensors of small magnetic fields.

The deposition of GMR films, including multilayers[67] and later also more advanced exchange biased sandwich stacks[102] onto flexible substrates, was first demonstrated by Parkin *et al.* in 1992. The magnetoresistive performance of extended GMR layers deposited on flexible foils, including polyimide, polyethylene terephthalate, polyetherimide, and regular transparency, was found to be comparable to stacks on rigid SiOx wafers. Deformations of GMR sensoric structures were originally applied on conventional SiOx wafer or glass supports to study effects of inverse magnetostriction on the magnetoelectric characteristics[103] and eventually use those for highly sensitive strain gauges.[104,105] Although the supports used in these studies are considered rigid, they allow for a small amount of bending deformation, which is translated to the functional magnetic layers on the outer surface as a tensile deformation (bending strain) of the order of about 0.1%. Later, similar studies were performed using plastic polyimide substrates,[106] which allowed for magnetoelectric measurements at tensile strains of up to 0.75% directly applied by stretching.[107]

Higher levels of deformation were obtained by Chen *et al.*, who deposited extended GMR films on buffer coated polyester transparency, as shown in Figure 5(a).[68] No performance degradation was observed in the magnetoresistive elements after 1000 bending cycles to a radius of about
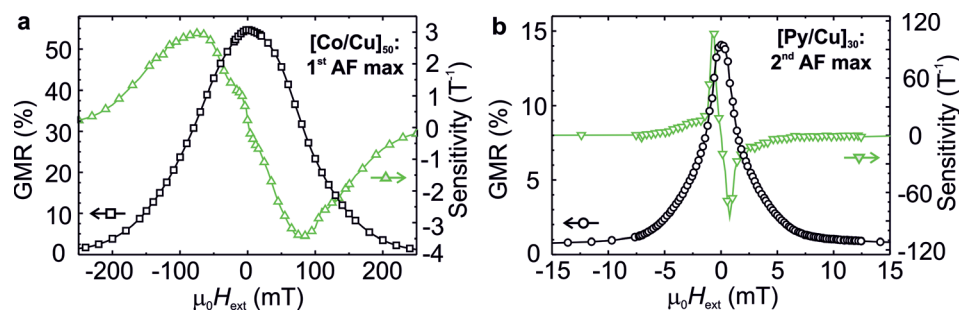

FIG. 4. GMR characteristics of Co/Cu multilayers: (a) GMR curve (black squares) and sensitivity (green triangles) of Co/Cu multilayers (Co(1 nm)/[Co(1 nm)/Cu(1.2 nm)]$_{50}$) coupled in the first antiferromagnetic (AF) coupling maximum. (b) GMR curve (black circles) and sensitivity (green triangles) of Py/Cu multilayers (Ni$_{81}$Fe$_{19}$(1.5 nm)/[Ni$_{81}$Fe$_{19}$(1.5 nm)/Cu(2.3 nm)]$_{30}$) coupled in the second antiferromagnetic coupling maximum. Reproduced with permission from Melzer *et al.*, RSC Adv. **2**, 2284 (2012). Copyright 2012 The Royal Society of Chemistry.
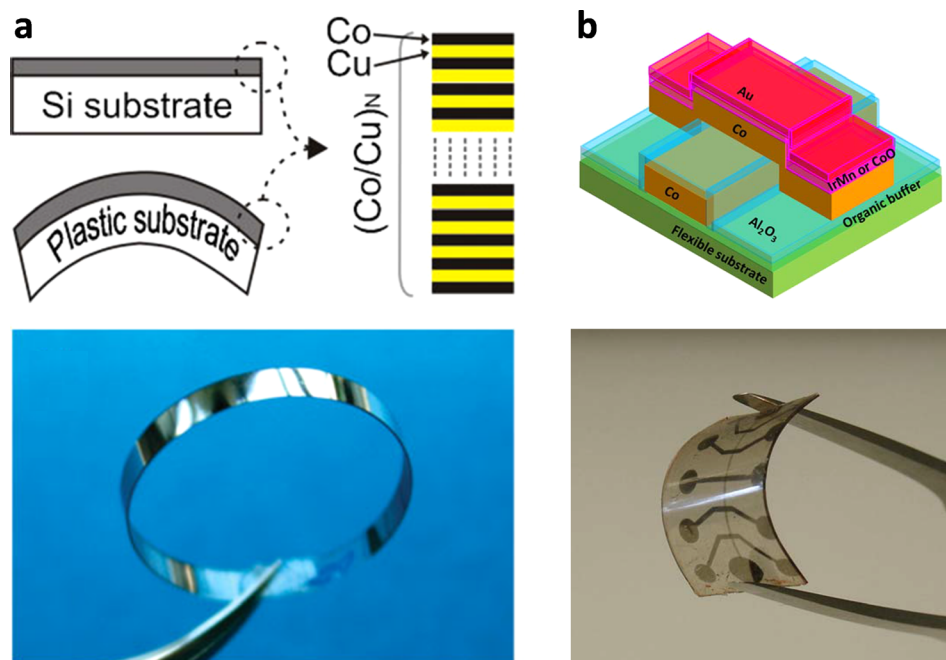
FIG. 5. Flexible magnetoelectronics: Magnetic sensoric systems on bendable polymeric foils. (a) GMR multilayers. Reprinted with permission from Chen *et al.*, Adv. Mater. **20**, 3224 (2008). Copyright John Wiley & Sons, Inc. (b) Magnetic tunnel junctions. Reprinted with permission from Appl. Phys. Lett. **96**, 3 (2010). Copyright 2010 AIP Publishing LLC.

22 mm. Furthermore, tensile testing of the flat GMR film up to above 2% strain revealed a mechanism for a mechanical fine tuning of the magnetoelectric properties.

Even high-performance TMR elements were successfully prepared on flexible polymeric supports,[69,108] which is highly challenging due to the necessary incorporation of smooth tunnel barriers in the low nanometer thickness regime into the device structure (Figure 5(b)). Although being slightly differed from the reference devices on rigid SiOx wafer, the magnetoelectric response in the flat state was unaffected by bending the sensors to a radius of 15 mm and back.[69]

1. Technological relevance

Flexible magnetic sensorics with high sensitivity bears potential to revolutionize the field of modern medical research. Indeed, magnetic nanoparticles are broadly utilized in, i.e.,

early diagnostics or therapeutics of cancer, point of care tests, immunological bioassays, and manipulations of biospieces. To bring state-of-the-art biomedical diagnostic devices to the hands of the people in need, a primary task is to reduce the price of the devices and allow for their high-volume delivery in a cost efficient manner, e.g., container transportation. For the latter, a crucial aspect is to reduce the weight of the device, which can be achieved by fabricating complex multifunctional devices on polymeric foils.[12,32,41,79,109] To this end, a highly flexible high performance microfluidic magnetic device with an integrated continuous microfluidic flow system was recently demonstrated (Figure 6).[70] The entire device can be bent down to a radius of 2 mm, still maintaining its full performance, i.e., fluidic characteristics and magneto-electrical response, which renders it the most flexible microfluidic analytic tool reported so far. The limit of detection for the magnetic contents in an emulsion droplet of 1 nl is about 4 mg/ml. This is perfectly suited for the identification of emulsion droplets that can be produced for

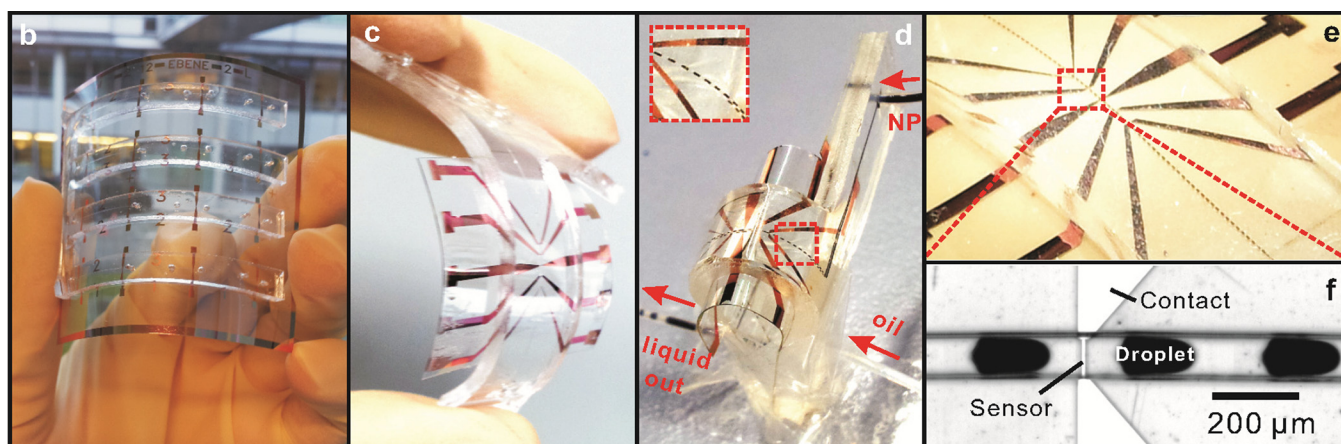FIG. 6. A highly flexible GMR-based analytic device filled with liquid and producing emulsion droplets on chip. Magnification of the part marked with a red rectangle on the chip. The real time detection of a train of emulsion droplets with encapsulated magnetic nanoparticles which are passing across the sensor. Reprinted with permission from Lin *et al.*, Lab Chip **14**, 4050 (2014). Copyright 2014 The Royal Society of Chemistry.

full-range magnetic manipulations of droplets on-chip, which can be beneficial for bioassays, drug discovery, and disease diagnostics. A strong advantage of the developed platform on light weight 100-μm-thick flexible foils over conventional electronics fabricated on rigid substrates is the possibility of a large area fabrication and adaptivity by redesigning the final product on demand. For instance, a single working unit on a flexible foil can be cut out, or redundant parts of the support for specific applications can be removed simply by cutting. Furthermore, the devices on polymeric support are about 10 times lighter compared to their rigid counterparts realized on conventional 500-μm-thick Si wafers, which makes them cost efficient for high-volume delivery to medical institutions or point-of-care distribution centers worldwide.

C. Magnetoimpedance sensorics

Magnetic field sensorics has benefited from the discovery of a new effect in *magnetically coated non-magnetic microwires* known as the giant magneto-impedance (GMI).[88–91] The GMI effect resembles itself as large variation of the real and imaginary part of the complex sensor impedance, driven with an alternating current (AC), when exposed to a magnetic field. GMI devices operate at room temperature[90,110] and reveal remarkable sensitivity to small magnetic fields down to pico-Tesla regime.[91,111–115] Although the GMI effect does not have a long history, it is already implemented in devices applied in the automotive, space, and medical sectors.[113,116] Thin film fabrication technologies emerged as an integrated circuit friendly alternative to the wire based technology, potentially allowing the fabrication of sensor arrays.[117,118] The NiFe/Cu/NiFe stacks are chosen as model prototype GMI systems, revealing a stable effect with an amplitude in the range of 100%/Oe below 100 MHz excitation frequency and characteristics suitable for lab investigations.[119,120]

Due to their simple structure and high magnetic sensitivity, GMI sensors are promising candidates for flexible magnetic sensing applications.[72,193] Recently, a novel method relying on strain engineering to realize arrays of on-chip integrated GMI sensors equipped with pick-up coils.[193] The geometrical transformation of an initially planar layout into a

tubular three-dimensional architecture with bending diameter of 50 μm only stabilizes favorable azimuthal magnetic domain patterns hence boosting the GMI effect 80 times offering remarkable sensitivity of 45 μV/Oe at excitation current of 1 mA. This work creates a solid foundation for further development of CMOS compatible GMI sensorics for magneto-encephalography. Furthermore, $Ni_{80}Fe_{20}/Cu/Ni_{80}Fe_{20}$ trilayers with thicknesses of 100 nm/200 nm/100 nm (Figure 7(a)) were recently prepared on flexible Kapton substrates with a thickness of 125 μm (Figure 7(b)) by Li *et al.*[72] The sensors are characterized in a wide range of frequencies and under different bending conditions. The highest GMI ratio achieved is 90% at 1.1 GHz, when the sensor is bent down to a radius of 7.2 cm resulting in 299 MPa of compressive stress along the sensor. Two peak values of 5.2%/Oe and 9.2%/Oe are found as the sensitivity at 0.5 GHz and 1.1 GHz, respectively. The obtained magnetoresistance ratio and sensitivity show the advantage of the magneto-impedance (MI) sensor in terms of their magnetic sensing performance over flexible GMR sensors, reaching magnetoresistance ratios of about 50% and a sensitivity in the range of 1%/Oe.

1. Technological relevance

MI/GMI sensors could be utilized in a wireless fashion, e.g., through integration with surface acoustic wave devices[121] on flexible substrates to obtain passive and wireless magnetic sensing devices.[122] For wireless applications, magnetic sensors working in the high frequency region (GHz) are favorable as the device and antenna size are inversely proportional to the operating frequency. In order to demonstrate the applicability of the flexible MI sensor, the effect of the Earth's magnetic field on the sensor's orientation was measured. This is, for instance, relevant for motion or orientation sensing in flexible, wearable devices. The impedance sinusoidally changes from 6.05 Ω to 6.13 Ω, where the peak values correspond to the sensor alignment being parallel or antiparallel with the Earth's magnetic field (Figure 8). The inset shows the magnetic field characteristic of the sensor at 500 MHz and under a 5 Oe bias field, which is characterized by a linear response in a field range from 5 Oe to −5 Oe.
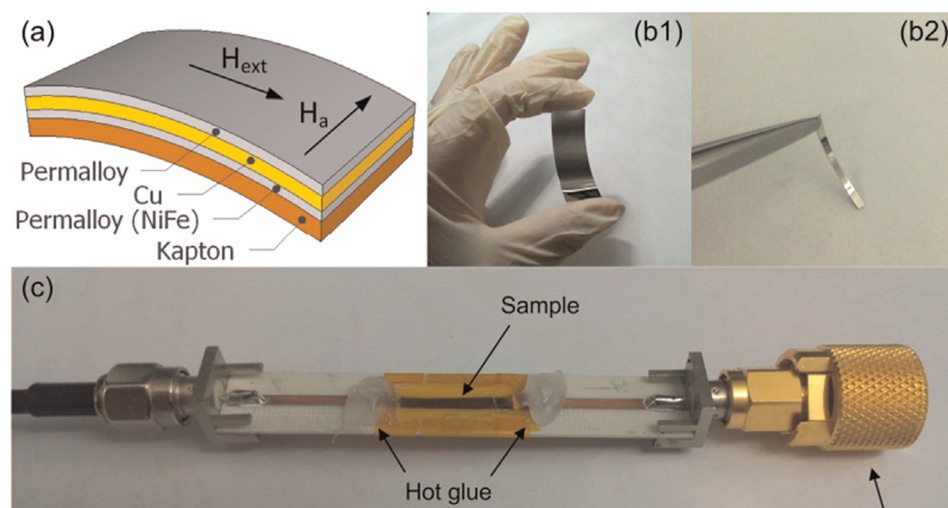
FIG. 7. Flexible GMI sensor element on Kapton: (a) The layer stack of a sensor on a Kapton substrate. (b1) A layer stack deposited on a flexible Kapton substrate. (b2) GMI sensor strip of 22 mm × 1.5 mm after patterning. (c) Picture of the flexible GMI sensor mounted on the sample holder. (d) Schematic of the high-frequency microstrip-based deflection measurement setup for the flexible magnetic sensor. Reprinted with permission from Li *et al.*, J. Magn. Magn. Mater. **378**, 499 (2015). Copyright (2015) Elsevier.

FIG. 8. Orientation of the flexible GMI sensor in the Earth magnetic field: Impedance of a flexible magnetic sensor as a function of the orientation, when rotated by 360°. The sensor is operated at 500 MH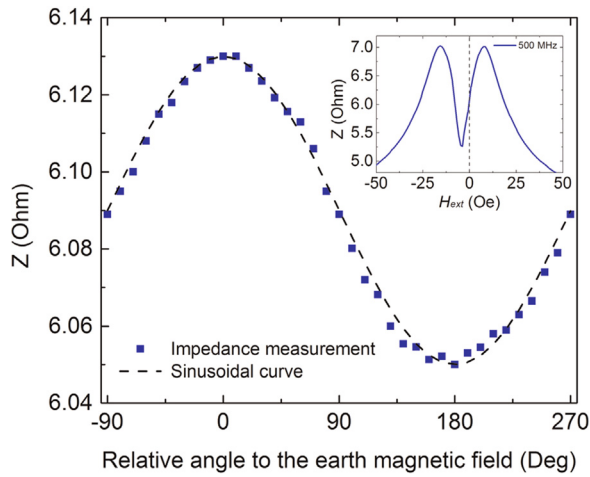z and 5 Oe bias field. Inset: impedance characterization of the sensor at 500 MHz and 5 Oe bias field. Reprinted with permission from Li *et al.*, J. Magn. Magn. Mater. **378**, 499 (2015). Copyright (2015) Elsevier.

D. Further development directions

The integration of these flexible sensing elements prepared on polymeric support with on-site signal conditioning electronics is challenging. This, however, is crucial for high precision sensorics in environments with electromagnetic disturbances. This issue could be overcome by combining high-performance sensorics with thin Si membranes accommodating integrated CMOS circuitry. Very recently, the performance of GMR multilayered magnetic sensors realized on thinned Si membranes was reported.[73] It was shown that the thinning down to 50 μm thickness of the Si support renders enough flexibility to attain bending radii down to 6.8 mm, keeping the GMR ratio of the sensors unchanged at a value of $(15.3 \pm 0.4)\%$. Mechanical and magnetic stability has

been proven with cyclic bending experiments. We discuss the observed behavior of the magnetic sensors regarding their applicability on flexible Si based integrated circuits[3,123] either as magnetic switches or as magnetic field sensors.

This demonstration potentially enables converting these flexible high-performance magnetosensors into stretchable devices relying on the rigid islands approach. This relies on distributed functional elements or clusters prepared on arrays of rigid islands, which are attached to an elastic carrier and electrically linked by highly stretchable interconnects,[124,125] as shown in Figure 9(a). These systems resemble a mesh layout with functional nodes and are mostly fabricated using transfer printing techniques.[126] Upon stretching, the compliant electrical bridges accommodate the lateral deformation, e.g., by means of wrinkling or meander shapes, while the functional islands ideally remain unstrained and just increase their distance to each other (Figure 9(b)). Hence, it is possible to directly convert established electronic architectures to stretchable systems[13,42,127] without relying on thin film based electronic components. This motivates the fabrication of a variety of highly functional and stretchable systems using approaches raging from integrated circuitry,[128] electronic eye cameras,[129] light emitting diodes[14] (Figure 9(c)), batteries,[37] as well as on-skin thermal[28] and implanted physiological sensors.[51] In most cases, the metallic interconnects are encapsulated between two flexible polymer sheets, as shown in Figure 9(d), to increase their yield strength. Also, a similar design of reversely compliant electronic mesh structures relying on free standing plastic foil without the use of elastomeric materials has recently been demonstrated.[10] The potential of this technology for stretchable magnetic sensorics is still to be explored.

III. PRINTABLE MAGNETIC SENSING DEVICES

Flexible devices strongly benefited from the recent developments of organic[12,131,132] as well as inorganic[41,133]
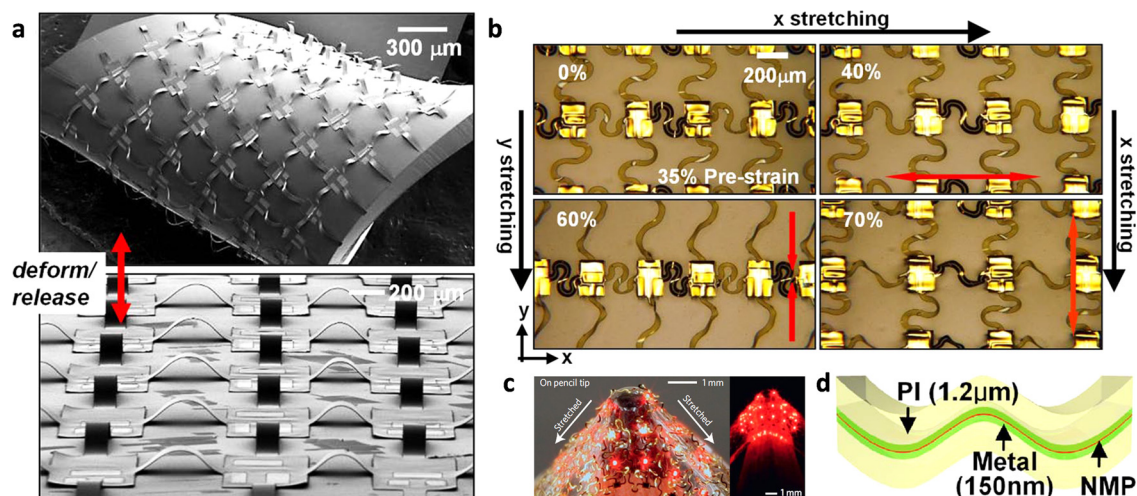

FIG. 9. Stiff islands with compliant interconnects for stretchable electronics: (a) Array of stiff islands housing CMOS inverters linked by buckled interconnects on an elastic support, in a twisted (top) and flat (bottom) state. (b) A similar array using more compliant serpentine bridge designs as interconnects stretched in the x- and y-direction. (a) and (b) Reprinted with permission from Kim *et al.*, Proc. Natl. Acad. Sci. U. S. A. **105**, 18675 (2008). Copyright 2008 The National Academy of Sciences of the U.S.A. (c) 6 × 6 array of μ-LEDs in a mesh design stretched on a pencil tip. Reprinted with permission from Kim *et al.*, Nat. Mater. **9**, 929 (2010). Copyright 2010 Macmillan Publishers Ltd. (d) Encapsulation of the electronic interconnects between two thin polymer sheets of polyimide (PI) close to the neutral mechanical plane (NMP). Reprinted with permission from Appl. Phys. Lett. **93**, 044102 (2008). Copyright 2008 AIP Publishing LLC.[130]

electronics, which are prepared using printing and/or thin film technologies. Being synergetically combined with either inkjet, screen, or dispenser printing approaches, flexible electronics has witnessed fascinating innovations in several application areas, including but not limited to displays,[134] organic light-emitting diodes (OLEDs),[135] various types of sensors,[74,76,136–139] radio frequency identification (RFID) tags,[140,141] and organic solar cells.[142] To complete the family, there are strong activities towards the fabrication of flexible magnetic field sensorics envisioning active intelligent packaging, post cards, books, or promotional materials that communicate with the environment when externally triggered by a magnetic field.[43,74–76,79]

The fabrication of printable magnetoelectronics is challenging, mainly due to the lack of suitable sensing compounds at ambient conditions. Indeed, in order to be in line with the concept of printable electronics, the magnetic ink should satisfy the following basic requirements: low-cost, high-volume production on large areas of standard printing materials, disposability, and processability. In this respect, it is known that magnetic nanoparticles surrounded by a non-magnetic matrix reveal various spin-dependent transport phenomena.[98,143,144] Thus, they may act as magnetoresistive sensor devices potentially enabling realization of printable magnetoresistive sensorics. Depending on the material of the interparticle matrix, different effects may occur: while insulating materials result in TMR, the use of conducting matrices leads to GMR effects.

A. Nanoparticle-based magnetic tunnel junctions

Here, assemblies of pure metallic magnetic nanoparticles made of Co, Fe, Ni, or their alloys are used, stabilized by an organic shell, which is adjusted to act as a tunnel barrier.[145] Tan *et al.* showed that chemically synthesized, ligand stabilized nanoparticles can be used for a bottom-up preparation of granular TMR systems.[144,146] TMR magnitudes of up to 3000% at low temperatures have been reported in such granular three-dimensional self-assembled supercrystals consisting of FeCo nanoparticles. Only very recently, room-temperature TMR was observed[147] in assemblies of fully metallic cubic Fe nanoparticles, with a mean size of about 9 nm, surrounded by hexadecylamine $[CH_3(CH_2)_{15}NH_2]$/hexadecylammonium $[CH_3(CH_2)_{15}NH_3{}^+Cl^-]$. Measurable resistances of the devices were ranging from 5 to 6 MΩ at room temperature. The

magnitude of the TMR is 0.9% and 0.3% at 2 K and 300 K, respectively. Although TMR at room temperature is demonstrated, its small magnitude is not yet fully optimized for applications in printable magnetoelectronics.

B. Nanoparticle-based giant magnetoresistive (GMR) sensors

Weddemann *et al.*[148] investigated the transport properties in two-dimensional monolayers of 8 nm Co nanoparticles embedded in a conducting matrix. After the self-assembly process, the insulating ligand shells were removed by heating the particles in a reducing gas atmosphere. Subsequently, a thin Cu layer was deposited on top of the nanocrystals. The magneto-electrical characterization of the samples at room temperature revealed a GMR effect with a magnitude of about 4%. Despite the promising GMR response, the resistance of the samples is too large (about 100 MΩ) due to their small thickness, which is inappropriate for applications in printable magnetoelectronics. Furthermore, the orientations of magnetic moments in such two-dimensional assemblies are correlated along domains with an antiparallel orientation. Consequently, the evolution of the magnetic configuration and magnetoelectric response strongly depends on the history of the magnetic pattern and repeated measurements made under identical conditions result in significantly deviating responses, which is unacceptable for magnetic field sensorics.[148]

Recently, Meyer *et al.* reported a GMR of up to 260% at room temperature for granular systems consisting of carbon-coated Co nanoparticles of 18 nm in diameter, embedded in conductive gel-like non-magnetic matrices (Figure 10(a)).[149] The magnitude of the GMR effect and the switching behavior of the particle-gel mixture was found to be dependent on the density of magnetic nanoparticles in the direction of the external field (Figure 10(b)). The large magnitude of the GMR effect is promising to realize printable magnetic field sensors. However, the system also reveals a large hysteresis (difference of the magnetoresistance curves taken in the increasing and decreasing magnetic fields; Figure 10(a)), which makes it difficult to apply the developed composites in their present form as magnetic field sensors. Furthermore, the choice of gels for the conductive matrix imposes limitations on thermal stability of the sensing elements for industrial temperature demands in range from −25 °C up to +85 °C.
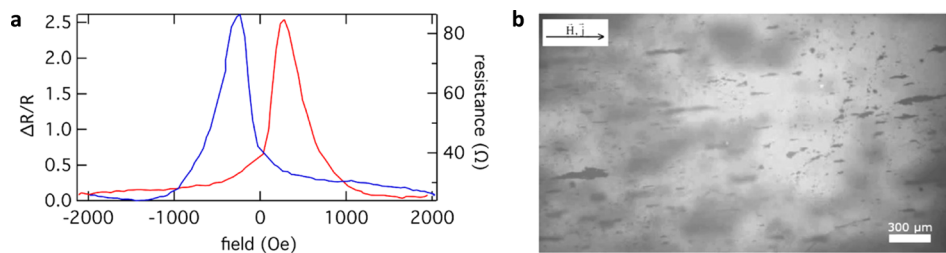

FIG. 10. Giant magnetoresistive gel composite: (a) GMR measurement obtained with Co nanoparticles in a conductive water-based gel matrix. The red curve indicates measurement with increasing, and blue with decreasing, field. (b) Optical microscopy image of the sample after measuring GMR response. The large darker areas can be attributed to either unevenness in the substrate surface or agglomerates above the focus of the microscope. With the external field, stable chain fragments have evolved. Macroscopic particle chains over the entire sample length were not observed. Reproduced with permission from Meyer *et al.*, Smart Mater. Struct. **22**, 5 (2013). Copyright 2013 IOP Publishing.
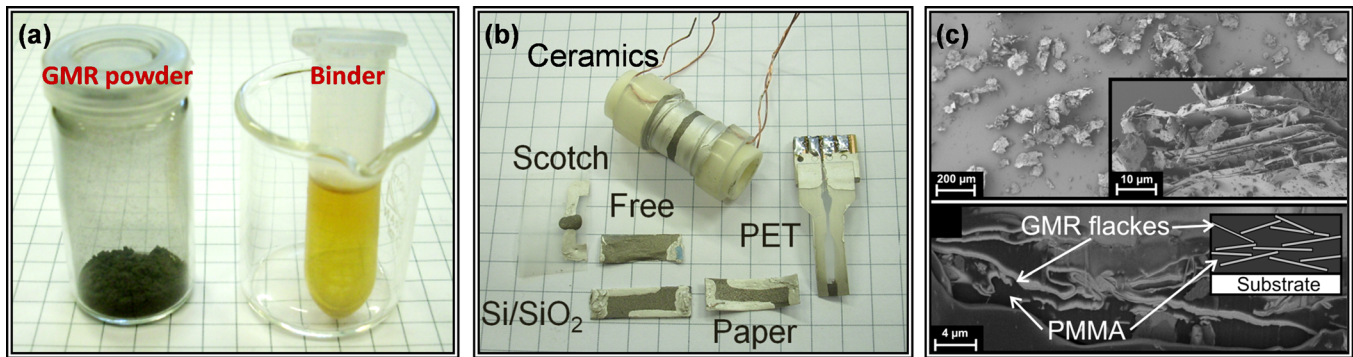
FIG. 11. Magnetosensitive paste for printable GMR sensorics: (a) Preparation of a GMR paste: GMR powder has to be mixed with a binder solution. (b) GMR paste can be painted on different substrates. (c) Top view scanning electron microscopy (SEM) image of the magnetic powder consisted of variously shaped flakes. The higher electrical conductivity is observed due to stacking of separate Co/Cu flakes (inset). SEM image of a cross-section through the printed sensor showing the internal structure of metallic flakes percolated inside polymer. (Inset) The schematic drawing demonstrates the principle of flake percolation. Reprinted with permission from Karnaushenko *et al.*, Adv. Mater. **24**, 4518 (2012). Copyright 2012 John Wiley & Sons, Inc.

C. Printed GMR devices

To overcome the above mentioned issues and to realize printable magnetic sensorics relying on the GMR effect, printable magneto-sensitive pastes were developed,[74] which are prepared using standard sputter deposition together with milling and mixing processes. The use of standard fabrication methods demonstrates the suitability of this kind of printable devices for large scale industrial production. Fabrication in brief: GMR stacks of a total thickness of 110 nm consisting of $50 \times$ [Co(1.0 nm)/Cu(1.2 nm)] bilayers are grown on top of a polymer buffer layer prepared on a rigid wafer. After deposition, the samples are rinsed in acetone to release the GMR stacks from the substrates; the multilayered metal film flakes are then filtered out from the collected solvent, dried, and ball milled. The resulting powder is filtered through a grid that defines the maximum lateral size of a GMR flake in the range from 40 to 150 μm. A magneto-sensitive paste is prepared by mixing the GMR powder with a polymeric binder solution (Figure 11(a)). This paste can be applied using conventional brush painting or dispenser printing onto virtually any support, e.g., rigid wafers, paper, plastic foils (Figure 11(b)), or conventional FPC board, Figure 12(a). By thorough optimization of the polymeric binder, electrical percolation can be achieved between the GMR flakes (Figure 11(c)) and the sensors reveal up to 37% change in the electrical resistance in a magnetic field with a maximal sensitivity of 0.93 T^{-1} at 130 mT.[76] These figures are

comparable to the performance of conventional GMR sensors prepared using advanced thin film fabrication and patterning technologies. Furthermore, being printed at pre-defined locations on flexible circuitry the sensors remain fully operational over a temperature range from $-10\,^\circ$C up to $+95\,^\circ$C, well beyond the requirements for consumer electronics (Figure 12).[76] This remarkable performance is unique to the proposed technology platform, which allows overcoming the main hurdle on the way towards commercialization of printable magnetic field sensorics, namely, its limited temperature stability due to the use of polymeric matrices.

With these specifications, printed magnetoelectronic devices could be applied as passive components for flexible electronics responding to a magnetic field. Indeed, the output signal of the sensors can be conditioned using available printed[132,150] and flexible[41,133,151] active electronics. In combination with flexible and printable active electronics as well as wireless communication modules,[140,141] the high performance magnetic field sensors enable the realization of complex platforms capable of detecting and responding to an external magnetic field. This feature is of great interest to realize smart packaging and energy efficient magnetic field driven switches.[74]

1. Technological relevance: Printed GMR-based switch

To demonstrate the functionality of a painted GMR sensor element on a proof-of-concept level, the sensor is
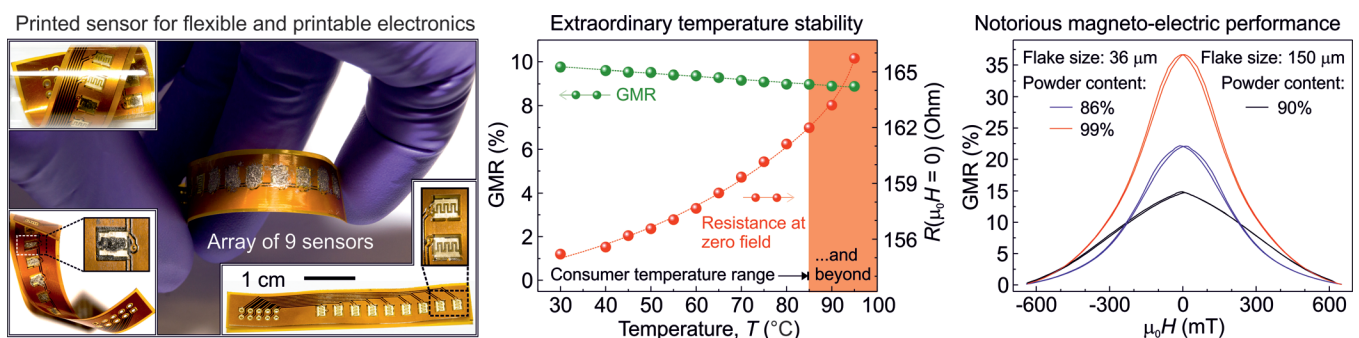
FIG. 12. Printed GMR sensors for flexible electronics: (a) Flexible and printable high performance magneto-sensorics prepared on a conventional flexible printed circuit board. The printed device reveals extraordinary temperature stability even beyond the requirements for consumer electronics (b) and magneto-electric performance up to 37% (c), which is comparable to their rigid counterparts, prepared using advanced thin film fabrication technology. Reprinted with permission from Karnaushenko *et al.*, Adv. Mater. **27**, 880 (2015). Copyright 2015 John Wiley & Sons, Inc.

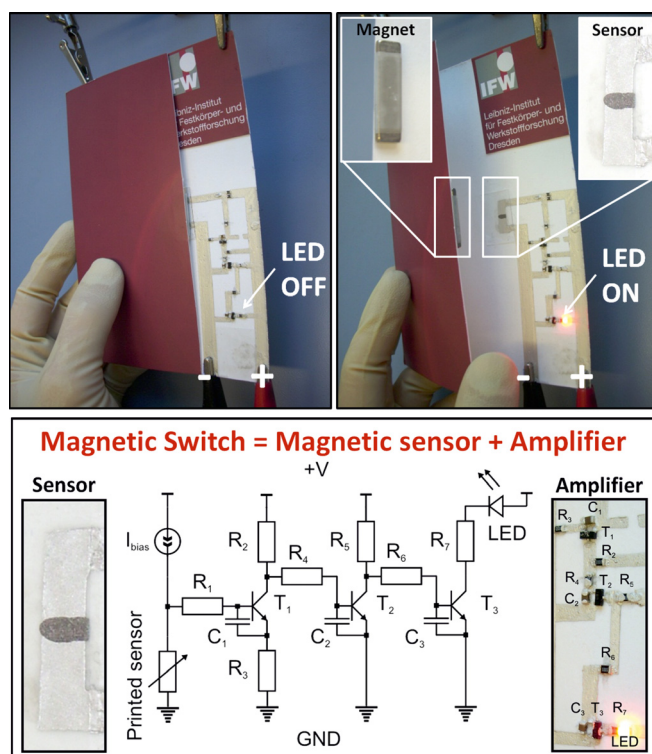FIG. 13. Magnetic field driven switch for printable electronics: (top) the printable sensor is integrated in a hybrid electronic circuit (amplification cascade with an LED) fabricated on the paper of a postcard. The LED ON/OFF state is triggered by a magnet that modifies the resistance of the sensor. This change of resistance alters the open/close state of the transistors in the amplifier regulating the current through the LED. (Bottom) Magnified view of the electronic circuit with the printed sensor. The circuit contains a current source I_{bias} to bias the sensor, a three stage amplification cascade with transistors T_1–T_3, resistors R_1–R_7, and capacitors C_1–C_3. The last amplification cascade supplies the LED. Adapted with permission from Karnaushenko *et al.*, Adv. Mater. **24**, 4518 (2012). Copyright 2012 John Wiley & Sons, Inc.

integrated in an electronic circuit fabricated directly on the paper of a postcard (Figure 13, top panel).[74] Conductive silver paste was used to paint interconnects. For demonstration, we chose a hybrid circuit consisting of painted elements (interconnects and sensor) combined with conventional solid state discrete transistors, capacitors, resistors, and an LED. When the postcard is closed, the LED is switched off. Opening the postcard switches the LED on. The ON/OFF state of the LED is triggered by a small permanent magnet that modifies the resistance of the printable magnetic sensor. This change in resistance, in turn, alters the open/close state of the transistors in the amplification cascades on the postcard (Figure 13, bottom panel) regulating the current flow through the LED. Note that all these discrete elements (resistors, transistors, diodes) used for electronic circuitry as well as the permanent magnets are available for printable electronics.[152] Therefore, the fabrication of a fully printable circuit with an integrated magnetic sensor is possible.

D. Further development directions

A large scale industrial application of this technology requires a high-volume production of the magneto-sensitive inks, which will be proven to be printable using industrially standard printing methods. With respect to the first aspect,

an approach could be envisioned based on electrochemical deposition of GMR multilayers,[153] which offers advantages for an upscaling of production at a competitive price with respect to thin film fabrication techniques. To address the second issue, at the present development stage of the technology, it seems most feasible to realize printing using direct write dispenser devices, which allow for versatile adjustments of the printing parameters. The achievable lateral sizes and thicknesses of the printed GMR sensors depend on the viscosity of the GMR paste. Working parameters and viscosity values shall be identified for homogeneous coverage of the substrate, and a minimal amount of GMR powder needed to produce a printed GMR sensor. As the costs of the printed GMR sensors are mainly determined by the production costs of the GMR powder, this analysis will provide an estimation of the price per sensor or price per area.

IV. STRETCHABLE MAGNETOELECTRONICS

In order to be able to elastically stretch GMR sensor elements to high levels of tensile deformation, the magnetic nanomembranes should be situated on an elastomeric (rubber) substrate. The accommodation of high strains in thin films of intrinsically stiff materials can be facilitated by morphologic features,[154] e.g., wrinkles,[155] which have to be introduced into the device system. They are able to transfer large tensile deformations of the substrate into minimal strains in the functional film.[156,157]

A. GMR multilayers on polydimethylsiloxane (PDMS)

The feasibility of magnetoresistive thin films on elastomeric supports was investigated by preparing lithographically structured GMR multilayers of Co(1 nm)/[Co(1 nm)/Cu(1.2 nm)]$_{50}$ were sputter deposited directly onto a film of PDMS, which was spin coated on a silicon handling wafer equipped with an anti-stick layer.[43] A resultant array of sensor elements is presented in Figure 14(a). In order to obtain specimens on free-standing stretchable membranes, the PDMS film was cut and then individual elements were peeled from the rigid silicon wafer, as shown in Figure 14(b). The final samples were free-standing 40 μm thick PDMS rubber membranes coated with photopatterned GMR multilayer structures (Figure 14(c)).

Figure 15(a) shows the field dependent GMR ratio measured at room temperature for such GMR multilayer elements on different substrates. The response curves obtained from samples prepared in the same deposition run on rigid silicon wafer without (SiOx) and with PDMS coating (PDMS/SiOx) are very similar. A maximum GMR value of more than 50% is obtained on both substrates, which is a typical value for Co/Cu based GMR multilayers.[158] Furthermore, the GMR characteristic does not change after the sample is peeled off the silicon wafer (PDMS). Hence, the magnetic sensing capabilities of GMR multilayer elements on free-standing rubber membranes are as good as on conventional rigid silicon substrates.[43] The absolute sensor resistances for the three cases, as given in the caption of Figure 15, are also found to be very comparable, as well.
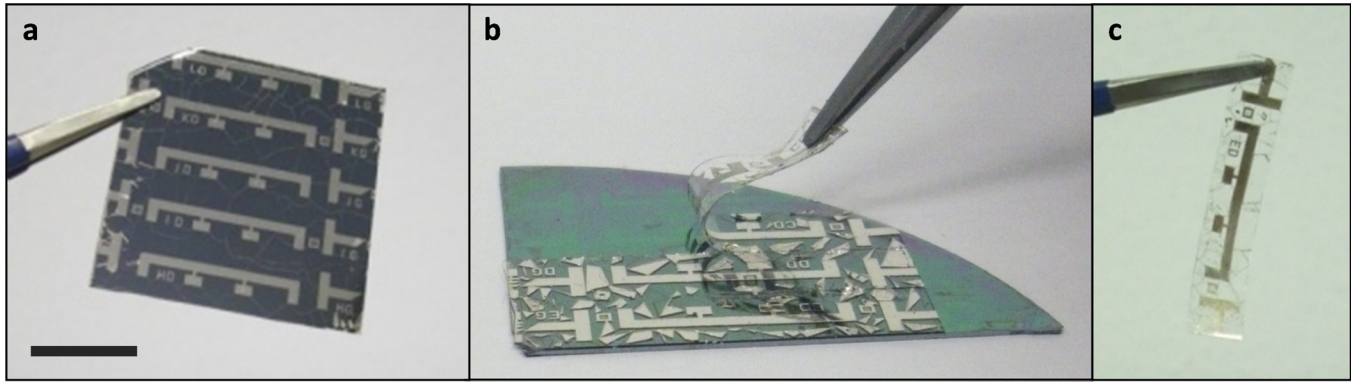
FIG. 14. Peeling of GMR multilayers on PDMS from the handling wafer: (a) Array of photopatterned Co/Cu multilayers on a PDMS coated silicon wafer (scale bar: 10 mm). (b) Peeling of an individual GMR element from the rigid silicon support by means of the anti-stick layer. (c) Photopatterned Co/Cu multilayer element on a free-standing PDMS membrane of 40 μm thickness. Reprinted with permission from Melzer *et al.*, Nano Lett. **11**, 2522. Copyright 2011 American Chemical Society.

Although the GMR performance of the devices on free-standing PDMS membranes and on PDMS-coated silicon wafers is similar, their morphology is found to be substantially different. Figures 15(b) and 15(c) show photographs and optical microscopy close-ups of a GMR multilayer on top of the PDMS surface before and after the rubber was released from the rigid substrate. When the rubber film is still attached to the silicon wafer, the metal film is smooth, which indicates low intrinsic stresses during the deposition of the GMR multilayers.[154] On the peeled rubber membrane, however, an extensive formation of buckles is observed (bottom of Figure 15(c)).

B. Morphology of the GMR sensor elements on PDMS

1. Surface wrinkling

A thin film of a stiff material deposited or laminated onto a pre-stretched elastomeric substrate, as illustrated in Figure 16(a), undergoes a morphologic transition by formation of periodic out-of-plane buckles, as the pre-strain is released.[159–161] This phenomenon is called *wrinkling*[155] and occurs as soon as a critical compressive strain is exceeded, which depends on the mechanical properties of both materials. Based on nonlinear analyses of the bilayer system, proposed by Huang *et al.*,[162] the critical strain ε_c for the formation of wrinkles can be computed by

$$\varepsilon_c = 0.52 \left[\frac{E_s \left(1 - \nu_f^2\right)}{E_f \left(1 - \nu_s^2\right)} \right]^{2/3} \tag{4.1}$$

via the Young's modulus E and Poisson's ratio ν of the substrate s and film f materials, respectively. This critical strain provides the energy necessary to form the out-of-plane distortions of the substrate and allow for film bending.

Figure 16(b) shows a 3D profile of a wrinkled gold film after uniaxial compression from 15% pre-strain. The wrinkling of hard skin on soft membranes exhibits a characteristic periodicity that scales with the thickness of the film. Bowden *et al.* suggested a model for the determination of the wrinkling period λ[159]
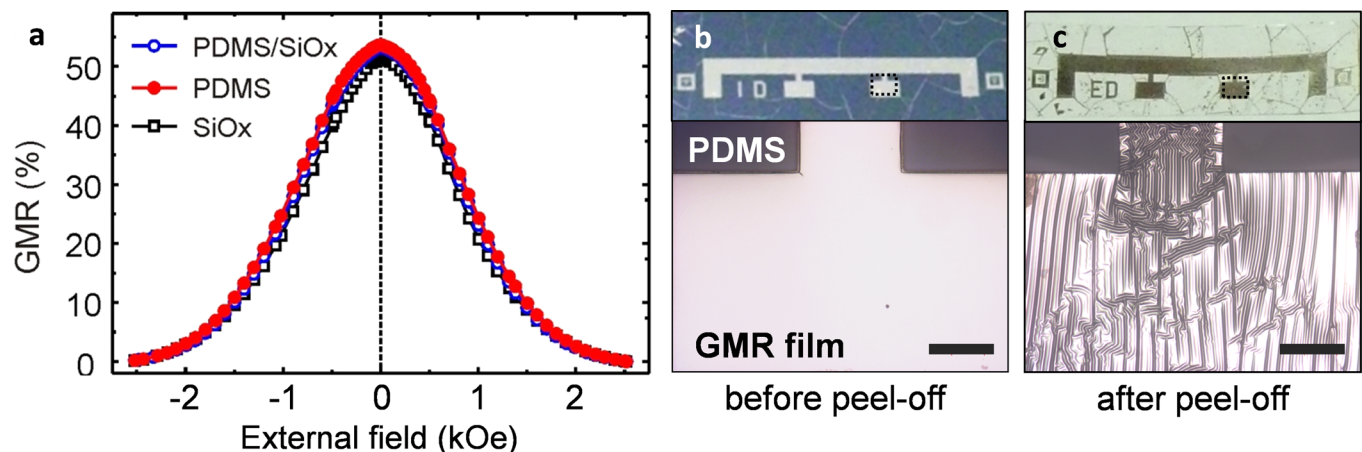

FIG. 15. Characterization of GMR multilayers on PDMS: (a) GMR curves of Co(1 nm)/[Co(1 nm)/Cu(1.2 nm)]$_{50}$ GMR elements on rigid silicon wafer (□; $R_0 = 15.3$ Ω), PDMS coated silicon wafer (○; $R_0 = 15.9$ Ω) and free-standing PDMS membrane (●; $R_0 = 15.0$ Ω). Even after the sample is peeled from the SiOx wafer, the GMR performance remains unchanged. (b) and (c) Photographs (top) of the PDMS/SiOx and PDMS samples, respectively, and optical micrographs (bottom) of the sections highlighted by the dashed squares. All scale bars: 200 μm. Reprinted with permission from Melzer *et al.*, Nano Lett. **11**, 2522. Copyright 2011 American Chemical Society.

FIG. 16. Wrinkle formation in stiff films on soft supports: (a) General fabrication scheme of a wrinkled metal film for stretchable electronics, by deposition onto a pre-stretched elastic support and subsequent release of pre-strain. (b) 3D profile of a wrinkled gold surface after release from 15% uniaxial pre-strain. (c) Biaxially wrinkled Si-based inverters on rubber, stretched and released in y- (top) and x-direction (bottom). Adapted with permission from Kim *et al.*, Science **320**, 507 (2008). Copyright 2008 AAAS.

$$\lambda = \frac{\pi d}{\sqrt{\varepsilon_c}} = 4.36 d \left(\frac{E_f \left(1 - \nu_s^2 \right)}{E_s \left(1 - \nu_f^2 \right)} \right)^{\frac{1}{3}}, \qquad (4.2)$$

with d being the thickness of the stiff film. This calculation holds for films firmly attached to a softer substrate with a thickness much larger than d. It only determines the initial wrinkling period upon reaching the critical strain, as with further shrinkage of the soft support, the wrinkles are compressed accordingly.

The described phenomenon can be exploited for stretchable electronic systems, because a wrinkled nanomembrane can accommodate tensile strains by levelling out its buckles.[156,163] In the ideal case, the film can be stretched until the original pre-strain is reached (i.e., the point where the film is flat again). According to investigations performed by Khang *et al.*, the lateral strains in the folded stiff film upon stretching are dominated by the bending, as long as the wavy pattern remains.[163] The peak strain can thus be approximated by

$$\varepsilon_f^{\text{peak}} = 2\varepsilon_c \sqrt{\frac{\varepsilon_{\text{pre}} - \varepsilon_{\text{appl}}}{\varepsilon_c} - 1}, \qquad (4.3)$$

with ε_{pre} and $\varepsilon_{\text{appl}}$ being the used pre-strain and currently applied strain on the substrate, respectively. The wrinkling approach also allows closed large area membranes to be stretched without cracking. Nevertheless, also other materials, which are not present as a closed film, like carbon nanotubes or other types of nanowires, can exhibit compliant properties using wrinkles.[24] Furthermore, it can lead to biaxial stretchability if the elastomeric substrate is pre-stretched in both lateral dimensions.[164] As shown in Figure 16(c), these features have led to the design of highly integrated stretchable electronic systems relying on surface wrinkling.[5,9,23,24]

2. Thermally induced wrinkling of GMR films

The observed wrinkling of the GMR layer upon peeling in Figure 15(c) results from the curing of the spin-coated PDMS films at an elevated temperature during its fabrication. The thermal shrinkage of the cured rubber film upon cooling down is suppressed in the lateral directions by the rigid silicon wafer it is attached to. This suppression is due to a large mismatch of the thermal expansion coefficients α of the two materials ($\alpha_{\text{PDMS}} = 9.6 \times 10^{-4}$ K^{-1} vs. $\alpha_{\text{Si}} = 2.6 \times 10^{-6}$ K^{-1}). As a result, a significant part of the thermal contraction of the rubber is "stored" by means of a compressive lateral stress arising inside the elastic PDMS film. This stress is maintained during the structuring and sputter deposition of the GMR layers and is not released until the sample is peeled from the rigid supporting wafer. Upon peeling, the rubber laterally contracts which causes wrinkling of the incompressible metal film.[161] This feature is referred to as *thermally induced wrinkling*.[164] The thermal contraction along one axis of the PDMS film for the applied temperature difference of $\Delta T = 70$ K (from 90 °C down to room temperature) is about 7%.

Figure 17(a) shows a 3D confocal laser scanning microscopy of the prepared GMR multilayer on a free-standing PDMS membrane. Although the thermally induced pre-strain leads to a laterally isotropic contraction of the rubber film, the wrinkles have a strong preference for a parallel alignment perpendicular to the photopatterned stripe structure (in Figure 17(a), the sensor stripe lies in the horizontal axis). This is expected, since wrinkles generally tend to align perpendicular to structural defects or the edges of structured films.[159,165] Furthermore, the specimens are peeled along the stripe structure, which favors the wrinkling perpendicular to it. The aligned wrinkling of the metal film, with the stress being relaxed along the sensor stripe, makes it stiffer in the orthogonal direction,[166] which prevents the perpendicular stress relaxation and associated wrinkling in most regions. Instead, a slight bending across the entire GMR stripe could be observed on the peeled sensor elements.

Wrinkling of hard films on soft membranes exhibits a characteristic period, which depends on the mechanical properties of both materials and scales with the film thickness.[159,167] The height profile of the soft GMR elements reveals a wrinkling period of $\lambda_{\text{exp}} = 19.7 \, \mu\text{m}$ and a mean
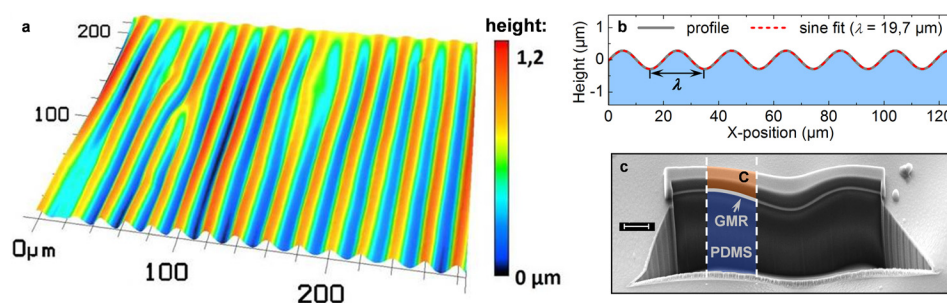
FIG. 17. Thermally induced wrinkling on PDMS: Wrinkled topology of GMR multilayer elements prepared on PDMS films after peel-off. (a) 3D confocal microscopy image showing the height profile. (b) Confocal line scan (gray) and sinusoidal fit (red) providing a mean wrinkle period λ of about 19.7 μm. (c) SEM image of a FIB cut through the sample showing the deposited carbon protective layer for FIB cutting, the GMR layer and the PDMS substrate (scale bar: 2 μm), Reprinted with permission from M. Melzer *et al.*, Nano Lett. **11**, 2522 (2011). Copyright 2011 American Chemical Society.

amplitude of about 0.45 μm (Figure 17(b)). A FIB cut of the sample (Figure 17(c)) discloses the wavy GMR film (indicated by the gray line) firmly attached to the bulky rubber (highlighted in blue). This suggests that the contact between the PDMS and the metal film is maintained throughout the wrinkle structure and no delamination occurs. As a result, we can apply the theoretical model suggested by Bowden *et al.*[159] to calculate the period of the wrinkles formed for a thin incompressible metal film of thickness d on an elastomeric surface, according to (4.2). The mechanical parameters used for the calculation are as follows: $E_s = 1.6$ MPa, $E_f = 171$ GPa ($E_{Co} \approx 211$ GPa, and $E_{Cu} \approx 131$ GPa, weighted by their respective share in the multilayer stack), $\nu_s = 0.48$, and $\nu_f = 0.33$ ($\nu_{Co} = 0.31$, $\nu_{Cu} = 0.35$). The Young's modulus of the PDMS was derived from stress-strain measurements,[43] while its Poisson's ratio and the data for the metal film are taken from the literature.[159,168,169] Considering the total thickness of the GMR multilayer stack ($d = 110$ nm), the calculation predicts a value for the wrinkling period of $\lambda_{theo} \approx 21.7$ μm, which is in good agreement with the experimental value derived from the line scan in Figure 17(b). The critical strain for the occurrence of wrinkling in the investigated system, according to (4.1), is computed to $\varepsilon_c = 0.26\%$.

C. Technological relevance: Magnetic detection on a curved surface

The prepared GMR elements on free-standing rubber membranes are thin and can easily conform to non-planar surfaces, which makes them interesting components for magnetic field measurements in curved geometries to provide information on the displacement of magnetized objects, e.g., tracking the angular position of the source of a magnetic field.[43] Furthermore, these novel magnetic sensors allow to introduce a conceptually new approach for the detection of magnetic objects flowing through a fluidic channel. It was shown that, due to their compliant nature, the elastic sensorics can be efficiently implemented in a millifluidic system by wrapping them tightly around the fluidic channel.[101] Given the imposed cylindrical symmetry, it is demonstrated that using this approach the stray fields generated by the flowing magnetic objects—e.g., magnetic particles, which are widely used for diagnostic or therapeutic purposes in biology and medicine[170–174]—can be detected virtually in all directions

(*isotropic sensitivity*),[101] which is unique compared to conventional rigid sensors.[82,175]

D. Stretchability test

According to the discussion above, the prepared GMR multilayer sensors are functional on curved surfaces. However, stretchable devices need to withstand *tensile deformations* as well. In this respect, the thermally induced wrinkling of the GMR layer on soft membranes can help to protect the metallic film from cracking and breaking by smoothing out the buckles during uniaxial elongation of the rubber substrate.[156] Flat metal films without surface wrinkling are expected to withstand tensile strains of below 1%.[176,177] In order to test the stretchability of the prepared sensor elements, a sample is mounted into a computer controlled GMR characterization setup with *in situ* stretching capability.[101] The measurement routine includes applying an external uniaxial strain to the sample and, for defined strain values, recording a GMR curve at room temperature, before the next stretching step is applied.

Figure 18(a) shows GMR curves for increasing strains applied to the multilayer element. All curves, according to the color chart in the legend, are plotted in the graph and are congruent to each other. Hence, the GMR characteristic remains unaffected by applied tensile deformations up to 2.5%. The data obtained during the stretching experiment are summarized in Figure 18(b), which displays the strain dependent GMR magnitude and absolute sample resistance of the sensor element during stretching. The curves show that the resistance remains constant for tensile strains below 1.7%. In this regime, the sensor can be regarded as *strain invariant*, as its signal can be directly correlated to an in-plane magnetic field without compensating for a resistance change due to the tensile deformation. With further stretching, the resistance rises strongly until the electrical conduction across the element is lost above 2.6%. This increase in resistance at higher strains is attributed to the formation of microcracks, which lower the cross section of the conducting metal film. The most striking aspect of the stretching experiment is that, although its absolute resistance is increasing by a factor of about 5 during the elongation, the GMR ratio remains at a constant level. Hence, as demonstrated with the matching GMR curves, this suggests that even if the metallic film is partly damaged by the imposed tensile strain, the
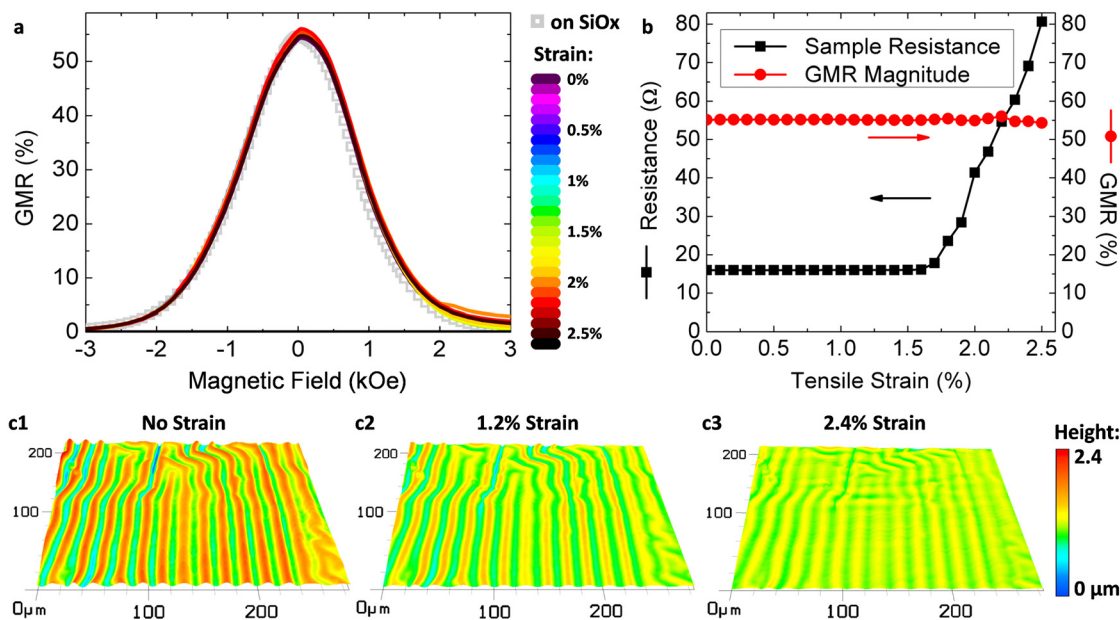
FIG. 18. Stretching test of a wrinkled GMR sensor on a PDMS membrane: (a) 27 GMR curves of a Co/Cu multilayer element measured at different applied strains (according to the legend) plus the reference curve recorded on a rigid SiOx wafer (□). (b) GMR magnitude (●) and sample resistance (■) in dependence of the imposed tensile strain. (c) 3D confocal microscopy images of the wrinkled GMR layer subjected to an increasing strain along the horizontal axis.

GMR effect is still present without major deterioration and the sample acts as a magnetic sensor element with the same performance as on rigid silicon substrates.[101]

Tensile strains imposed on magnetic multilayers are actually expected to influence the GMR effect by reducing the spacer thickness and thus varying the interlayer exchange coupling.[68,178] In the conducted experiment, however, no change in the GMR ratio upon stretching is found, which indicates that the tensile strain on the actual GMR multilayers is low due to the presence of the wrinkles. A set of confocal micrographs showing the wrinkled topology of the GMR film at zero strain and at two different stretched states is provided in panels (1–3) of Figure 18(c). With increasing strain, the wrinkles become less pronounced and the entire metal film becomes smoother.

E. Direct transfer printing of GMR sensorics

The above discussed approach to fabricate stretchable magnetoelectronics relies on the direct deposition and lithographic structuring of magnetoresistive thin films onto elastomeric membranes. However, this method is associated with severe process limitations, preventing significant advances in performance and level of complexity and thus restricting the applicability of the technology. First of all, the photolithographic structuring on the PDMS surface is challenging for feature sizes well below $100\,\mu m$ (Ref. [179]), and multiple patterning steps, which are absolutely necessary for the integration of magnetoelectronic components into multifunctional stretchable electronics platforms, can hardly be realized on PDMS reliably. Another crucial drawback is related to the limited stretchability of the functional elements relying on wrinkling due to a thermally induced pre-strain. In fact, stretchabilities of a few percent only[101,179] can be

achieved in this way, unless cracking of the sensing layer is permitted. Controlled cracking can result in higher stretchabilities, which was demonstrated also with magnetoelectronic sensing elements by means of stretchable spin valves.[77] However, stretching due to crack formation is applicable only for thin film elements that are much larger than the cracks, and hence, this approach contradicts the device miniaturization, which is highly relevant, especially for the integration into wearable navigation and orientation systems, bio-medical systems,[180,181] or for the fine mapping of inhomogeneous magnetic fields and textures.

For the fabrication of stretchable magnetic sensorics, a *single step transfer printing* process was developed.[78] Figures 19(a)–19(h) show the process flow of the developed direct transfer method for GMR multilayer sensor elements to uniaxially or biaxially pre-stretched PDMS membranes. Upon detaching the sensor device from the rigid handling wafer, the mechanically induced pre-strain is released, which leads to a wrinkling of the transferred structures on the PDMS rubber (Figure 19(i)). The strength of the plasma induced adhesion between the GMR multilayer and the PDMS membrane is demonstrated in Figure 19(j). The cross-section prepared using FIB etching shows that the GMR multilayer is firmly attached to the soft PDMS, even throughout the wrinkles. The wrinkled sensor elements on the soft support can be elastically stretched according to the induced pre-strain. *In situ* stretching experiments revealed a stable sensor performance up to about 30% of uniaxial strain applied to these GMR meanders.[78]

To highlight the main features enabled by the introduced transfer process, an array of micro-sized GMR sensors with electrical contacting was fabricated, which requires two-step lithography to be performed (Figures 20(a)–20(g)). For the sensor array, highly sensitive Py(1.5 nm)/[Py(1.5 nm)/
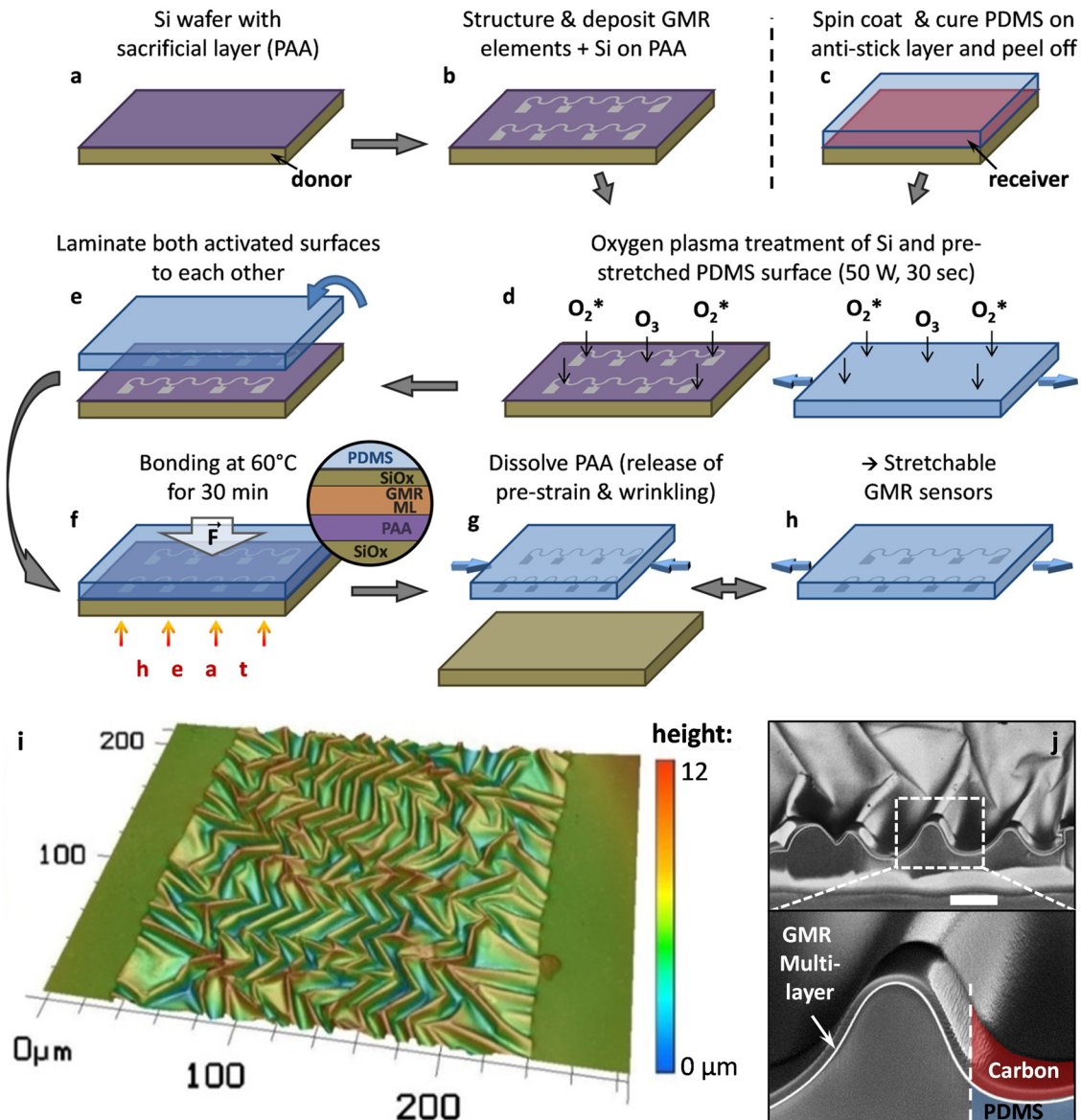
FIG. 19. The direct transfer preparation method. Process flow: (a) and (b) Preparation of GMR multilayers with a Si capping layer on a poly(acrylic acid) (PAA) coated Si wafer (donor). (c) Spin coating and curing of a PDMS film (receiver) on an anti-stick layer coated carrier. (d) Oxygen plasma activation of donor and pre-stretched receiver substrate. (e) and (f) Heat and pressure assisted adhesion of both activated surfaces. The magnified view in (f) shows a cross section of the bonding interface region. The bonding is established between the top Si surface, which is oxidized to SiO_x by the plasma and the activated PDMS (layers not drawn to scale). (g) Dissolving of the PAA sacrificial layer to detach the GMR structures from the donor substrate and release of the pre-strain in the receiver membrane to obtain a wrinkled morphology. (h) The transferred sensors can be elastically stretched in the direction of the pre-strain. (i) A confocal microscopy image showing the wrinkled topography of the transferred GMR multilayer element using a biaxial pre-strain of 25% × 25%. (j) SEM images of a FIB cut through the transferred GMR film showing the good adhesion of the wrinkled magnetic nanomembrane to the PDMS support (scale bar: 5 μm). Reprinted with permission from Melzer *et al.*, Adv. Mater. **27**, 1333 (2015). Copyright 2015 John Wiley & Sons, Inc.

Cu(2.3 nm)]$_{30}$ multilayers and a uniaxial pre-strain of 20% along the sensor stripes was used, as indicated in Figure 20(f). In the case of uniaxial pre-strain, the transverse direction has to be pre-stretched as well, in order to compensate for the Poisson's contraction, avoiding the destruction of transferred structures upon strain release. The final sensor array can be applied to any curved or soft surfaces, as demonstrated in Figure 20(h) with the GMR microsensors situated on a fingertip. The functionality of the transferred sensors is proven by GMR measurements on the meander element before and after the transfer process (Figure 20(i)). Both curves show a similar GMR signal with high sensitivities for small magnetic fields.

F. Further development directions

The sensor layout utilized in the present work was designed as a test structure for the establishment of stretchable GMR sensorics that allows for precise magnetoelectric characterization. Since photolithographic patterning of the magnetoresistive nanomembranes was successfully applied from the very beginning, the device structure can be adapted and scaled to meet the requirements for specific applications and design concepts. Patterning defined meander structures, for instance, will adapt the electrical parameters of individual sensing elements to the requirements of a specific signal processing electronics. Preparing the GMR elements into a
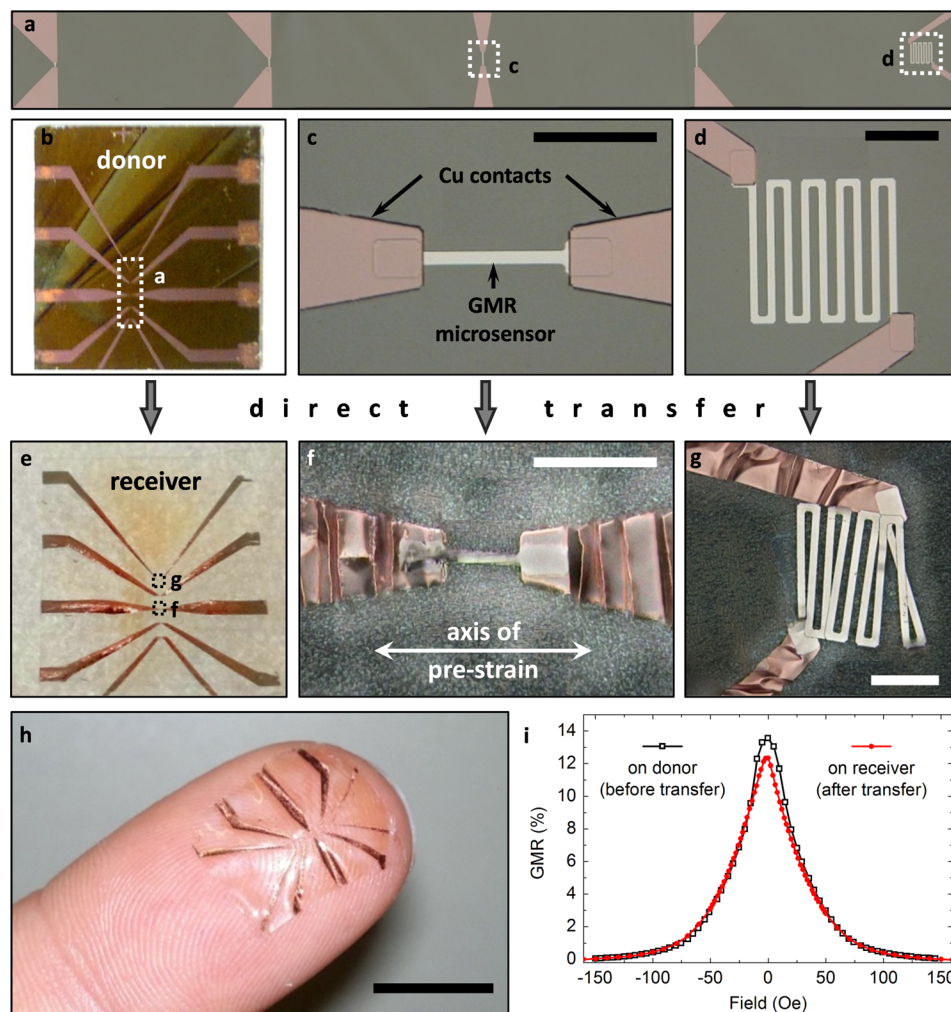
FIG. 20. Direct transfer of a GMR microsensor array: (a) Microscope image of the array of five $[Py/Cu]_{30}^{2^{nd}}$ GMR elements (four stripes of different length and one meander, widths: 6 μm). (b) Entire structure including contacts on the rigid donor substrate. (c) and (d) Magnified views of the 60 μm microsensor stripe and the meander with contacts to the electrodes, respectively. (e) and (g) Microsensors transferred to the receiving substrate using a uniaxial pre-strain of 20%, as indicated in (f). All scale bars: 50 μm. (h) The transferred microsensor array can conform to the soft and curved surface of a fingertip (scale bar: 10 mm). (i) GMR characteristics of the meander microsensor element before (■) and after (●) the transfer process. Reprinted with permission from Melzer *et al.*, Adv. Mater. **27**, 1333 (2015). Copyright 2015 John Wiley & Sons, Inc.

Wheatstone bridge configuration would allow for a differential signal and may compensate for temperature effects. An integration of compliant ferromagnetic structures[182] can help to realize a magnetic biasing of the proposed GMR sensors to operate them around a defined working point of the GMR response curve in a fully stretchable design. This would not only allow using the maximum sensitivity of the respective elements but may also add a sense of directionality to lift the symmetry of magnetic field sign in GMR multilayers. Finally, detailed finite element method (FEM) mechanical modeling will be necessary to further guide sensor improvements.

V. IMPERCEPTIBLE MAGNETOELECTRONICS

In order to go beyond the possibilities provided by using elastomeric membranes like PDMS as support for GMR thin films to obtain arbitrarily deformable sensing elements, the novel approach of *imperceptible electronics*[12] is exploited. Imperceptible electronics relies on the fabrication of functional thin film electronic elements on ultra-thin (<2 μm) polymeric membranes. The reduction in the flexible substrate to a minimum thickness imparts its thus gained mechanical properties of extreme bendability and light-weight to the entire electronic device.[12] Weight and flexibility are key figures of merit for large area electronics or robotic skin,[12,38] as they critically influence the mechanical response and

perception of the artificial system. The unique haptic character of functional electronic devices obtained using this approach allows for intimate contact with soft, biological tissue or organs, and complex, arbitrarily shaped 3D free forms. Both organic and inorganic electronic components were very recently introduced in this respect. Besides electronic circuitry,[41] also tactile sensors,[12] light emitting diodes,[21] solar cells,[32] as well as thermoelectric elements[29] have been realized. The here reviewed imperceptible magneto-sensitive elements readily conform to ubiquitous objects, which paves the way to go beyond the imitation of natural skin functionalities and could equip the recipient with the "*sixth sense*" *of magnetoception*.[183,184] Magnetoception is a sense which allows bacteria, insects, and even vertebrates like birds and sharks to detect magnetic fields for orientation and navigation.[183,184] Humans are however unable to perceive magnetic fields naturally. Magnetosensorics is a versatile tool to assess orientation or mechanical movements that should become wearable on-skin and may also be operated *in vivo* in order to add magnetoception to our natural cognition. Such advanced applications require very specific mechanical properties of the sensing elements, such as bending radii smaller than 10 μm, stretchabilities exceeding 100%, as well as a sensitivity for magnetic fields below 100 Oe. Such a compliant nature makes magneto-electronic devices ideally suited also for wearable, yet unobtrusive and imperceptible orientation and manipulation aids.
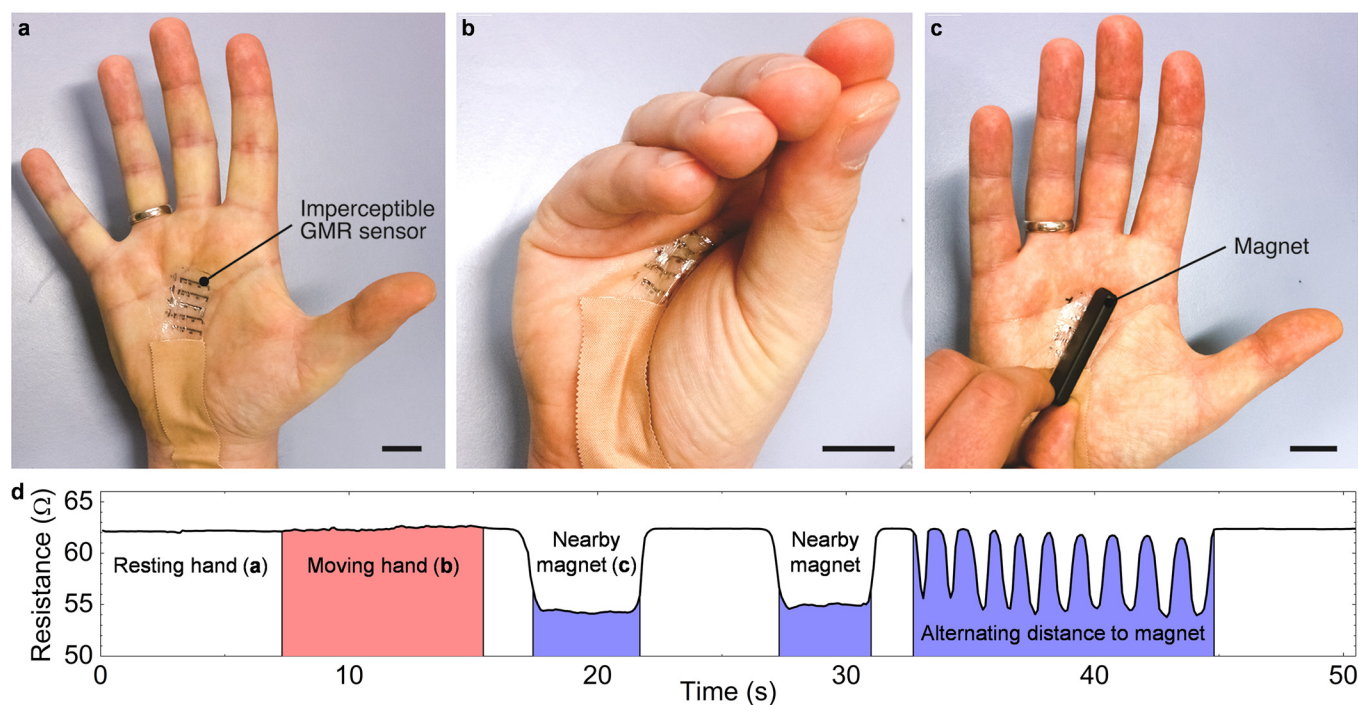
FIG. 21. Imperceptible GMR sensors: (a)–(c) Imperceptible GMR sensor array on a human palm with one element connected to a readout circuit during rest, moving the hand and in proximity to a permanent magnet, respectively. All scale bars: 20 mm. (d) recorded resistance of the sensor element for panels (a)–(c). Reproduced with permission from Melzer *et al.*, Nat. Commun. **6**, 6080 (2015). Copyright 2015 Macmillan Publishers Ltd.

A. Imperceptible GMR sensor skin

GMR multilayer elements were fabricated on ultrathin poly(ethylene terephthalate) (PET) membranes with a thickness of 1.4 μm. Independent of the extreme thinness of the polymeric support, the sensor devices behave very similar to their rigid counterparts.[79] Imperceptible magnetoelectronic elements were readily worn directly on the palm of the author's hand as demonstrated in Figure 21. Here, a set of five GMR sensors intimately conforms to the inner hand and simultaneously follows the motions and deformations of the skin when the hand is moved (Figures 21(a) and 21(b)). The presented elements are denoted imperceptible, because their presence on the skin is haptically not perceived by the recipient. One sensor element is electrically contacted with thin copper wires and the resistance of the on-skin sensor is recorded while moving the fingers, opening and closing the hand, applying a magnetic field with a permanent magnet, and alternating the distance to the magnet (Figure 21(c)). The recorded signal plotted in Figure 21(d) shows a small, noise-induced fluctuation during the motion of the hand (which amounts to less than 0.3%), whereas the field of the approaching permanent magnet induces a strong resistance drop of about 13% at its nearest position. Altering the distance between the permanent magnet and the on-skin GMR element results in a corresponding change in the sensor's resistance.

B. Ultra-stretchable GMR sensors

Artificial skin components should not only be flexible, but also elastic and ideally even withstand high biaxial deformations. Although the used ultra-thin PET foil is hardly stretchable itself, imperceptible electronics offers an elegant route to facilitate very high levels of tensile strain without any sacrifices in device performance by a facile post-fabrication transfer step onto a pre-strained elastomer.[12,21,32]

Individual elements of imperceptible GMR sensor foil are laminated onto pre-stretched stripes of highly stretchable adhesive tape (VHB^{TM} 4905 F from 3 M), as illustrated in Figure 22(a). Here, large pre-strains of 600% were used for the fabrication of compliant devices. Optical microscopy and scanning electron microscopy (SEM) top view images provided in Figures 22(b) and 22(c), respectively, reveal the highly wrinkled topology of the sensors after the relaxation of pre-strain. The magneto-sensitive capabilities of the presented elements are not affected by the post-processing, as shown in Figure 22(d), on the example of a GMR multilayer device measured before and after the lamination and wrinkling on the VHB tape. The GMR elements are laminated face down to the pre-stretched VHB tape, which in turn acts as an encapsulation for the functional magnetic layer between the stretchable tape and the ultra-thin PET foil, as visualized by SEM imaging of the sample's cross-section (Figure 22(e)) prepared by FIB milling. The cross-sectional SEM images of samples prepared with a high uniaxial pre-strain presented in Figure 22(e) reveal that some parts of the magnetoresistive foil on the tip of the buckles are bent into radii of curvature of less than 3 μm, while the sensor not only remains functional, but also maintains its full performance.

The stretchability of the postprocessed sensor elements is investigated in a GMR characterization setup with *in situ* stretching stage. A top view of a mounted and contacted stretchable GMR sensing element in a relaxed (left) and the fully stretched state (right) is provided in Figure 23(a). The axis of the applied magnetic field is perpendicular to the sensor stripe (along the wrinkles). The recorded GMR curves at
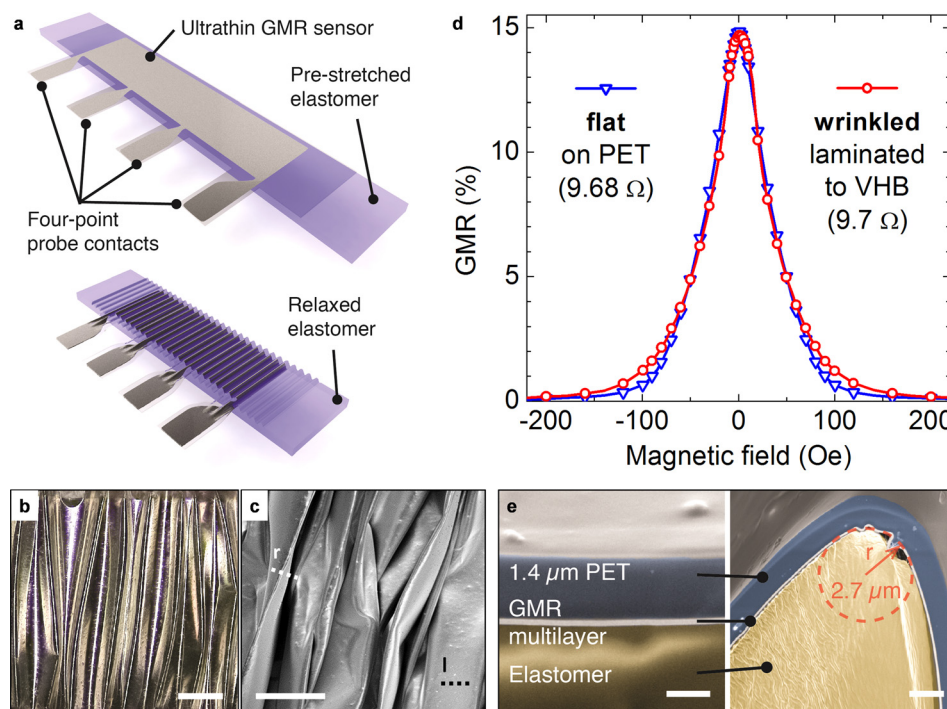
FIG. 22. Lamination of imperceptible GMR multilayers onto pre-stretched adhesive tape: (a) The post fabrication step to obtain ultra-stretchable GMR sensors from imperceptible elements by face-down lamination onto a highly pre-stretched stripe of VHB tape. Four contact pads are reaching beyond the tape (top). Relaxing the elastomer results in out-of-plane wrinkling of the sensor foil and enables re-stretching (bottom). (b) and (c) Optical microscopy (scale bar: 200 μm) and SEM (scale bar: 100 μm) top view images, respectively, revealing the wrinkled structure of the sensor surface in the relaxed state. (d) GMR curves of an imperceptible Co(1 nm)/[Co(1 nm)/Cu(2.2 nm)]$_{30}$ multilayer element at a flat state before lamination onto the pre-stretched VHB support ($\triangledown$) and at a highly wrinkled state after the release of pre-strain ($\bigcirc$). (e) Cross-sectional SEM images of a sensor foil laminated to the rubber tape. The GMR nanomembrane is encapsulated between the ultra-thin PET and the stretchable adhesive tape. Some parts of the magnetoresistive foil on the tip of the buckles are bent into radii of curvature of less than 3 μm (right). The location of cuts shown on the left and right is indicated in (c). Scale bars: 1 μm left and 2 μm right. Reproduced with permission from Melzer *et al.*, Nat. Commun. **6**, 6080 (2015). Copyright 2015 Macmillan Publishers Ltd.

different tensile strain levels up to 270% along the direction of pre-strain are congruent with each other, as presented in Figure 23(b). The progression of the GMR magnitude and the relative resistance change due to stretching of the sensor are plotted as a function of the uniaxial deformation in Figure 23(c). Both values also remain unchanged over this entire strain regime. At 270%, the PET foil with the GMR layer is fully elongated and the wrinkles vanish, as shown in the right hand picture of Figure 23(a). Confocal microscopy images of a sample at the maximum strain and just below are also included in Figure 23(d).

The here investigated magnitude of strain exceeds the typical demands for most on-skin and *in vivo* operations. It was also shown that the prepared GMR elements withstand extensive cyclic loading to high strains with no fatigue over 1000 cycles.[79] Furthermore, they could be prepared using biaxial pre-strain in order to accommodate large tensile deformations in both lateral dimensions simultaneously. The outstanding resilience of the presented imperceptible and stretchable GMR elements against high and repeated mechanical deformations can be attributed to the ductile properties of the used metals in the GMR stacks, in particular, those of copper. It has been recently shown that thin copper films are much less susceptible to aging upon repeated deformations in the concept of imperceptible electronics compared to, e.g., Al or Ag electrodes.[29]

1. Technological relevance

Magnetic field sensors can detect any type of motion. This feature allows us to position the imperceptible magneto-electronics as a magneto-sensory system for wearable electronics and electronic skin that equips the recipient with a "sixth sense" able to perceive the presence of static or dynamic magnetic fields or to precisely track its position in an artificial magnetic environment. Hence, these ultrathin magnetic sensors with extraordinary mechanical robustness are ideally suited to be wearable, yet unobtrusive and imperceptible orientation and manipulation aids.

Electronic skin on fingertips[185,186] is especially attractive for precise input and as communication interfaces due to our finger's fine motor skills. In Figure 24, an on-skin magnetic proximity sensor is demonstrated where a single imperceptible GMR element is attached to a fingertip and connected to a read out circuit. The presence of a magnetic field can thus be detected by simply pointing the finger towards it, and its strength is in this case visualized by an array of LEDs (Figures 24(a)–24(c)). Unlike optical sensors, no line-of-sight between the sensor and the magnetic field emitter is required. This allows transmitting "magnetic messages" through all non-magnetic objects like safety enclosures, displays, or even walls. The encoding can be realized both statically via permanent magnets as well as
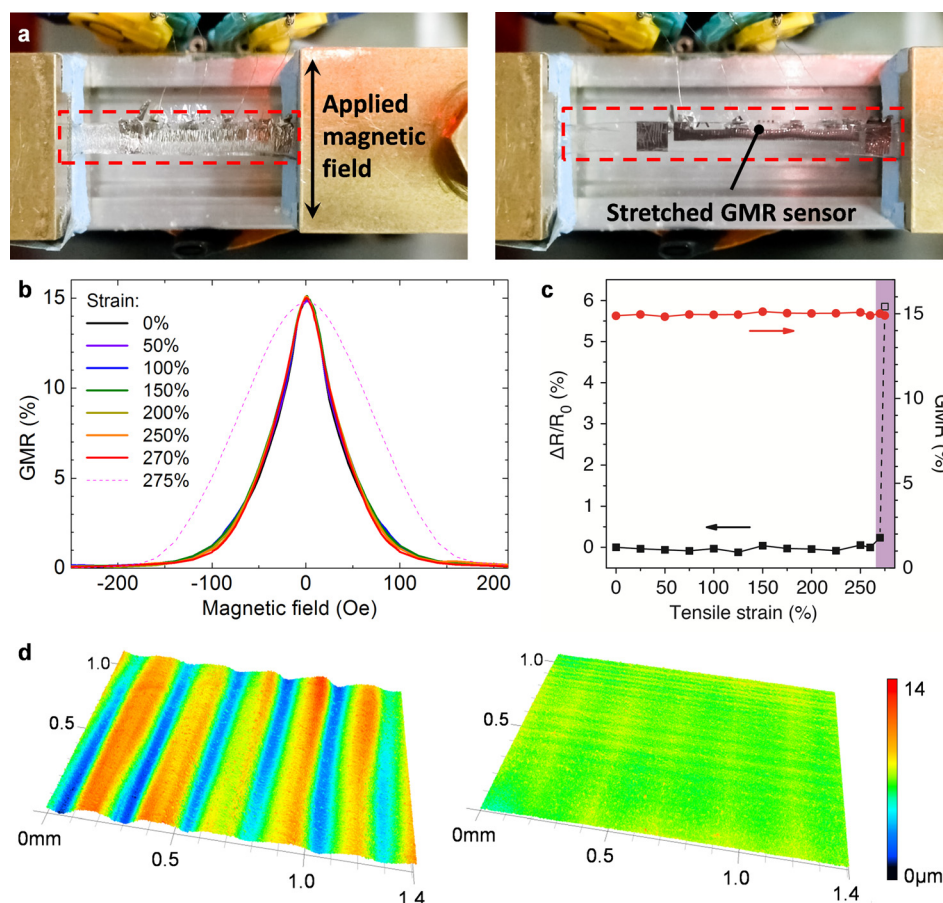
FIG. 23. Stretching of imperceptible GMR sensors: (a) A Co(1 nm)/[Co(1 nm)/Cu(2.2 nm)]$_{30}$ sample mounted to the *in situ* stretching stage relaxed (left) and fully elongated (right). The arrow in the left image indicates the axis of the applied magnetic field. (b) GMR curves recorded for strains from 0% to 250% in increments of 50%, plus 270% and 275%, according to the legend. (c) ● GMR magnitude and ■ resistance change normalized to 0% strain (R$_0$ = 9.7 Ω) as a function of applied strain. The shaded region indicates overstretching. (d) 3D confocal laser scanning micrographs showing the topology of the stretchable GMR sensors' surface (metalized side up) at a stretched state just before reaching the maximum strain (left) and precisely at the maximum strain, above which the resistance starts to increase (right). Reproduced with permission from Melzer *et al.*, Nat. Commun. **6**, 6080 (2015). Copyright 2015 Macmillan Publishers Ltd.

dynamically simply with current driven wirings. The demonstrated on-skin proximity detection system is a proof of concept for touch-less human-machine interaction relying on imperceptible magnetoelectronics. Similar approaches for motion and displacement sensorics are applicable for soft robots[56,187] as well as for magnetic functionalities in epidermal electronics.[38]

Imperceptible magnetoelectronics can be used also for biomedical applications, especially for the realization of functional medical implants.[47,51] In conjunctions with a magnetic field source, these imperceptible magnetoelectronics can be applied to monitor in real time the displacements of natural or artificial joints, as well as the expansion and contraction of muscles, e.g., the real time activity of the heart muscle to detect potential cardiovascular irregularities. The advantage would be to recognize potential health risks at early stages. When combined with wireless communication modules, these imperceptible magnetic sensorics can
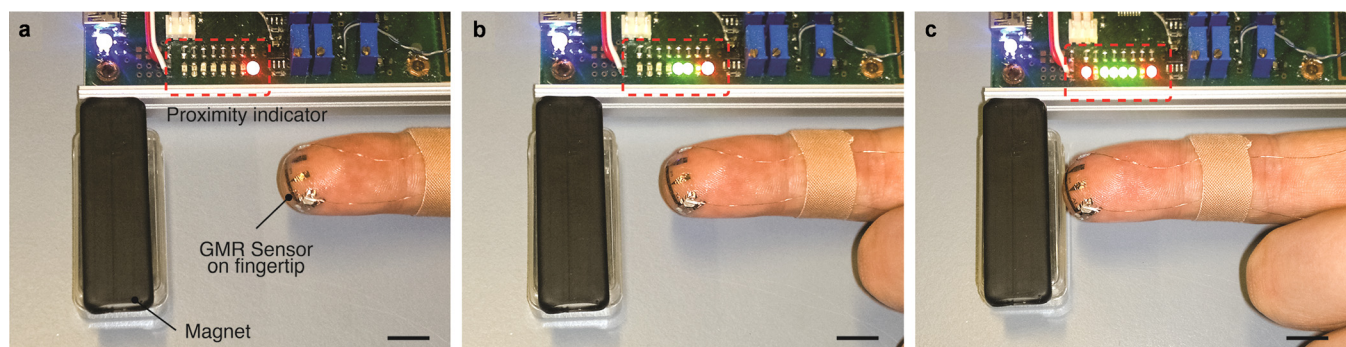

FIG. 24. Fingertip magnetic proximity detector: (a)–(c) Imperceptible sensor element on the fingertip connected to a linear array of LEDs (dashed red frame). All scale bars: 10 mm. Reproduced with permission from Melzer *et al.*, Nat. Commun. **6**, 6080 (2015). Copyright 2015 Macmillan Publishers Ltd.

provide immediate alerts to a mobile device or even warn medical doctors upon detecting muscle dysfunctions.

C. Further development directions

For a successful commercialization of imperceptible magnetic sensors, the long term stability upon deformation has to be verified. Further reliability tests against the persistent exposure to temperature changes, humidity, and vibrations have to be undertaken to qualify soft magnetic sensors for "real world" applications. To further reduce the impact of mechanical stresses on the functional magnetic nanomembrane upon device deformation, the GMR film may be situated in a neutral mechanical plane (NMP).[188] This can be realized by chemical vapor depositions of parylene, which results in a thin and inert passivation layer.[41] It homogeneously also covers highly non-planar surfaces with a controllable thickness and is even biocompatible.

VI. CONCLUSIONS

This review reflects the successful establishment of shapeable, namely, flexible, printable, stretchable, and even imperceptible magnetic sensorics, describing the currently available approaches from the first attempts verifying the functional concept to the realization of state-of-the-art highly compliant and strain invariant sensor devices with remarkable robustness. The developed technology platform offers considerable application potentials in the field of smart skins and textiles, soft robotics, medical implants, and consumer electronics. Since shapeable magnetoelectronics was demonstrated with different kinds of magnetosensitive systems, including Hall probes, various multilayers,[101] and spin valves,[77] it represents a universal basis for the realization of soft magnetic sensorics and may even be extended to advanced spintronic systems[189] (e.g., magnetoresistive memories[190] or magnetic logic devices[191]).

Future work should focus on optimizations to interface electrically and mechanically with other soft electronic components enabling, for example, signal conditioning,[41] multiplexing,[12] or wireless readout and remote sensing[38] to overcome the mayor issue of reliable electrical contacting. The integration of stretchable magnetoelectronics with various functional elements on comparable platforms, like solar cells,[32] light emitting diodes,[21] rechargeable batteries,[36] as well as temperature[29] and tactile[12] sensors, will enable autonomous and versatile soft smart systems with a multitude of sensing and responsive features.

A. Prospective applications

Several potential application areas of shapeable magnetic sensorics, i.e., electrical machines, wearable electronics, and smart skins; *intelligent* packaging; soft robotics; and medical implants, were already mentioned within the article. The dynamic detection of a soft diaphragm's actuation,[79] for example, demonstrates the high potential of stretchable magnetoelectronics for the emerging field of soft robotics[55,56] and elastomeric actuators.[22,57] Position and motion tracking in conventional machines and facilities (e.g., in automotive and production) is after all the main application area of magnetic sensorics, nowadays. Besides being cost efficient, this is mainly because on the emitting side (i.e., by means of permanent magnets) no power supply is needed, which also greatly enhanced the design freedom. The current establishment of soft robotic machines[59–61,63] calls for similar sensoric counterparts that share their novel mechanical properties. The stretchable GMR sensors reviewed here meet all the requirements, in particular, high sensitivity, strain invariance, and robustness, for the integration into soft robotic systems. However, in order to keep the entire system soft, the magnetic emitter should be compliant as well. Recently, Tseng *et al.* introduced stretchable designs of micromagnet arrays.[182] The intelligent incorporation of compliant
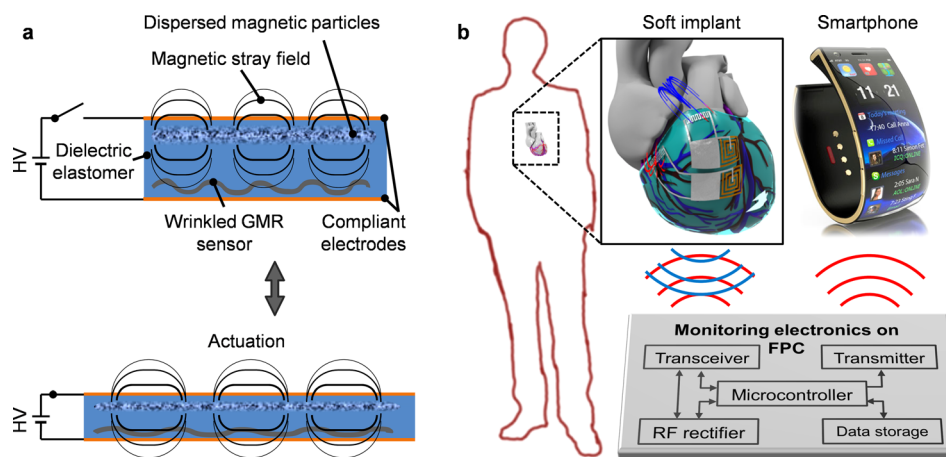

FIG. 25. Examples of prospective application: Conceptual view of two application examples for stretchable magnetoelectronics. (a) Integrated actuation gauge in a dielectric elastomer actuator (DEA). The DEA consists of a rubber dielectric film sandwiched between two compliant electrodes. Upon application of a high voltage, the electrostatic attraction of the electrodes squeezes the DEA, causing it to actuate laterally. The integrated stretchable GMR sensor detects a signal from the dispersed magnetic particles beneath the opposite electrode, due to their reduced distance upon actuation. (b) Smart medical implant for heart valve monitoring. Stretchable GMR sensors attached to the surface of the heart detect the motion of small permanent magnets implanted on the cardiac valves. Equipped with a wireless transmission module, it could automatically send an emergency call via the patient's mobile communication device, in the case of detected irregularities. Adapted from http://www.emopulse.com.

magnetic structures and stretchable GMR sensors into soft actuators, e.g., according to Figure 25(a), would allow for a highly integrated solution for detecting its deformations in real-time.

Furthermore, the demonstration of on-skin magnetoception[79] already enables magnetic proximity detection and will also allow for navigation and touchless control features in electronic skins. This work is foreseen to inspire a diverse number of e-skin devices that will benefit from a "sixth sense" magnetoception. The on-skin reception of "magnetic messages" transmitted through safety enclosures, for example, can have profound application potentials for high security environments. Passivated into biocompatible encapsulations, like parylene, the imperceptible sensor elements will also add the magnetic functionalities to medical implants[31] and advanced surgical tools.[51] The magnetic signal would need to come from artificial sources, like magnetic particles or small permanent magnets, being fixed onto the moving parts under surveillance. This would allow monitoring specific physiological actions and processes (e.g., joints or muscular and cardiac valve activity) and, for example, alert at imminent seizures (Figure 25(b)).

Finally, the successful realization of compliant arrays of microsized GMR sensors using the direct transfer approach renders high resolution magnetic mapping on arbitrary nonplanar surfaces possible. Similar investigations are by now only feasible on planar geometries, using optical or scanning probe techniques, or by means of synchrotron radiation. A GMR microsensor array, however, could perform real-time monitoring in a very compact configuration that allows the application also in an industrial environment. A multiplexing technique should necessarily be integrated into such a microsensory system, though, to account for an efficient data acquisition from numerous sensing elements.

ACKNOWLEDGMENTS

[1] S. R. Forrest, Nature **428**, 911 (2004).
[2] Y. G. Sun and J. A. Rogers, Adv. Mater. **19**, 1897 (2007).
[3] D. Shahrjerdi and S. W. Bedell, Nano Lett. **13**, 315 (2013).
[4] C. N. Hoth, P. Schilinsky, S. A. Choulis, S. Balasubramanian, and C. J. Brabec, in *Applications of Organic and Printed Electronics*, edited by E. Cantatore (Springer, New York, 2013), Vol. 1, p. 27.
[5] D. H. Kim *et al.*, Science **320**, 507 (2008).
[6] T. Sekitani, Y. Noguchi, K. Hata, T. Fukushima, T. Aida, and T. Someya, Science **321**, 1468 (2008).
[7] T. Someya, *Stretchable Electronics* (Wiley-VCH, Weinheim, 2013).
[8] T. Sekitani and T. Someya, Adv. Mater. **22**, 2228 (2010).
[9] D. J. Lipomi, B. C. K. Tee, M. Vosgueritchian, and Z. N. Bao, Adv. Mater. **23**, 1771 (2011).
[10] J.-H. Kim, M. J. Han, and S. Seo, J. Polym. Sci. Part B: Polym. Phys. **53**, 453 (2015).
[11] T. Someya, Y. Kato, T. Sekitani, S. Iba, Y. Noguchi, Y. Murase, H. Kawaguchi, and T. Sakurai, Proc. Natl. Acad. Sci. U. S. A. **102**, 12321 (2005).
[12] M. Kaltenbrunner *et al.*, Nature **499**, 458 (2013).
[13] D. H. Kim, J. L. Xiao, J. Z. Song, Y. G. Huang, and J. A. Rogers, Adv. Mater. **22**, 2108 (2010).
[14] R. H. Kim *et al.*, Nat. Mater. **9**, 929 (2010).
[15] S. Cheng and Z. G. Wu, Lab Chip **10**, 3227 (2010).
[16] M. Gonzalez, B. Vandevelde, W. Christiaens, Y. Y. Hsu, F. Iker, F. Bossuyt, J. Vanfleteren, O. van der Sluis, and P. H. M. Timmermans, Microelectron. Reliab. **51**, 1069 (2011).
[17] M. Park *et al.*, Nat. Nanotechnol. **7**, 803 (2012).
[18] H. Vandeparre, D. Watson, and S. P. Lacour, Appl. Phys. Lett. **103**, 204103 (2013).
[19] F. Cavallo and M. G. Lagally, Soft Matter **6**, 439 (2010).
[20] Z. B. Yu, X. F. Niu, Z. T. Liu, and Q. B. Pei, Adv. Mater. **23**, 3989 (2011).
[21] M. S. White *et al.*, Nat. Photonics **7**, 811 (2013).
[22] R. Pelrine, R. Kornbluh, Q. B. Pei, and J. Joseph, Science **287**, 836 (2000).
[23] X. Li, T. L. Gu, and B. Q. Wei, Nano Lett. **12**, 6366 (2012).
[24] D. J. Lipomi, M. Vosgueritchian, B. C. K. Tee, S. L. Hellstrom, J. A. Lee, C. H. Fox, and Z. N. Bao, Nat. Nanotechnol. **6**, 788 (2011).
[25] T. Yamada, Y. Hayamizu, Y. Yamamoto, Y. Yomogida, A. Izadi-Najafabadi, D. N. Futaba, and K. Hata, Nat. Nanotechnol. **6**, 296 (2011).
[26] M. Ramuz, B. C. K. Tee, J. B. H. Tok, and Z. N. Bao, Adv. Mater. **24**, 3223 (2012).
[27] H. C. Ko *et al.*, Nature **454**, 748 (2008).
[28] R. C. Webb *et al.*, Nat. Mater. **12**, 938 (2013).
[29] M. Drack, I. Graz, T. Sekitani, T. Someya, M. Kaltenbrunner, and S. Bauer, Adv. Mater. **27**, 34 (2015).
[30] O. Graudejus, Z. Yu, J. Jones, B. Morrison, and S. Wagner, J. Electrochem. Soc. **156**, P85 (2009).
[31] D. H. Kim *et al.*, Nat. Mater. **10**, 316 (2011).
[32] M. Kaltenbrunner, M. S. White, E. D. Glowacki, T. Sekitani, T. Someya, N. S. Sariciftci, and S. Bauer, Nat. Commun. **3**, 770 (2012).
[33] T. G. McKay, B. M. O'Brien, E. P. Calius, and I. A. Anderson, Appl. Phys. Lett. **98**, 142903 (2011).
[34] Y. Qi, J. Kim, T. D. Nguyen, B. Lisko, P. K. Purohit, and M. C. McAlpine, Nano Lett. **11**, 1331 (2011).
[35] M. Lee, C. Y. Chen, S. Wang, S. N. Cha, Y. J. Park, J. M. Kim, L. J. Chou, and Z. L. Wang, Adv. Mater. **24**, 1759 (2012).
[36] G. Kettlgruber, M. Kaltenbrunner, C. M. Siket, R. Moser, I. M. Graz, R. Schwodiauer, and S. Bauer, J. Mater. Chem. A **1**, 5505 (2013).
[37] S. Xu *et al.*, Nat. Commun. **4**, 1543 (2013).
[38] D. H. Kim *et al.*, Science **333**, 838 (2011).
[39] S. W. Hwang *et al.*, Science **337**, 1640 (2012).
[40] S. Bauer and M. Kaltenbrunner, ACS Nano **8**, 5380 (2014).
[41] G. A. Salvatore, N. Munzenrieder, T. Kinkeldei, L. Petti, C. Zysset, I. Strebel, L. Buthe, and G. Troster, Nat. Commun. **5**, 2982 (2014).
[42] J. A. Rogers, T. Someya, and Y. G. Huang, Science **327**, 1603 (2010).
[43] M. Melzer, D. Makarov, A. Calvimontes, D. Karnaushenko, S. Baunack, R. Kaltofen, Y. F. Mei, and O. G. Schmidt, Nano Lett. **11**, 2522 (2011).
[44] V. J. Lumelsky, M. S. Shur, and S. Wagner, IEEE Sens. J. **1**, 41 (2001).
[45] S. Wagner, S. P. Lacour, J. Jones, P. H. I. Hsu, J. C. Sturm, T. Li, and Z. G. Suo, Physica E **25**, 326 (2004).
[46] M. L. Hammock, A. Chortos, B. C. K. Tee, J. B. H. Tok, and Z. A. Bao, Adv. Mater. **25**, 5997 (2013).
[47] D. H. Kim *et al.*, Nat. Mater. **9**, 511 (2010).
[48] J. Viventi *et al.*, Nat. Neurosci. **14**, 1599 (2011).
[49] T. Ware, D. Simon, D. E. Arreaga-Salas, J. Reeder, R. Rennaker, E. W. Keefer, and W. Voit, Adv. Funct. Mater. **22**, 3470 (2012).

[50]G. Park *et al.*, Adv. Healthcare Mater. **3**, 515 (2014).

[51]D. H. Kim *et al.*, Proc. Natl. Acad. Sci. U. S. A. **109**, 19910 (2012).

[52]S. Gong, W. Schwalb, Y. W. Wang, Y. Chen, Y. Tang, J. Si, B. Shirinzadeh, and W. L. Cheng, Nat. Commun. **5**, 3132 (2014).

[53]K. Cherenack, C. Zysset, T. Kinkeldei, N. Münzenrieder, and G. Tröster, Adv. Mater. **22**, 5178 (2010).

[54]C. Zysset, T. Kinkeldei, N. Münzenrieder, L. Petti, G. Salvatore, and G. Tröster, Text. Res. J. **83**, 1130 (2013).

[55]F. Ilievski, A. D. Mazzeo, R. E. Shepherd, X. Chen, and G. M. Whitesides, Angew. Chem.-Int. Ed. **50**, 1890 (2011).

[56]R. F. Shepherd, F. Ilievski, W. Choi, S. A. Morin, A. A. Stokes, A. D. Mazzeo, X. Chen, M. Wang, and G. M. Whitesides, Proc. Natl. Acad. Sci. U. S. A. **108**, 20400 (2011).

[57]S. Schuhladen, F. Preller, R. Rix, S. Petsch, R. Zentel, and H. Zappe, Adv. Mater. **26**, 7247 (2014).

[58]G. Kofod, W. Wirges, M. Paajanen, and S. Bauer, Appl. Phys. Lett. **90**, 081916 (2007).

[59]R. V. Martinez, A. C. Glavan, C. Keplinger, A. I. Oyetibo, and G. M. Whitesides, Adv. Funct. Mater. **24**, 3003 (2014).

[60]R. V. Martinez, J. L. Branch, C. R. Fish, L. H. Jin, R. F. Shepherd, R. M. D. Nunes, Z. G. Suo, and G. M. Whitesides, Adv. Mater. **25**, 205 (2013).

[61]S. A. Morin, R. F. Shepherd, S. W. Kwok, A. A. Stokes, A. Nemiroski, and G. M. Whitesides, Science **337**, 828 (2012).

[62]C. Keplinger, T. F. Li, R. Baumgartner, Z. G. Suo, and S. Bauer, Soft Matter **8**, 285 (2012).

[63]B. Mosadegh *et al.*, Adv. Funct. Mater. **24**, 2163 (2014).

[64]C. Keplinger, J. Y. Sun, C. C. Foo, P. Rothemund, G. M. Whitesides, and Z. G. Suo, Science **341**, 984 (2013).

[65]C. Zysset *et al.*, Opt. Express **21**, 3213 (2013).

[66]See http://smarttextiles.se/en/saturday-light-fever-2/#prettyPhoto for further information on smart textiles, 2015.

[67]S. S. P. Parkin, K. P. Roche, and T. Suzuki, Jpn. J. Appl. Phys. Part 2: Lett. **31**, L1246 (1992).

[68]Y. F. Chen, Y. F. Mei, R. Kaltofen, J. I. Mönch, J. Schumann, J. Freudenberger, H. J. Klauss, and O. G. Schmidt, Adv. Mater. **20**, 3224 (2008).

[69]C. Barraud *et al.*, Appl. Phys. Lett. **96**, 072502 (2010).

[70]G. G. Lin, D. Makarov, M. Melzer, W. P. Si, C. L. Yan, and O. G. Schmidt, Lab Chip **14**, 4050 (2014).

[71]M. Melzer *et al.*, Adv. Mater. **27**, 1274 (2015).

[72]B. D. Li, M. N. Kavaldzhiev, and J. Kosel, J. Magn. Magn. Mater. **378**, 499 (2015).

[73]N. Perez, M. Melzer, D. Makarov, O. Ueberschär, R. Ecke, S. E. Schulz, and O. G. Schmidt, Appl. Phys. Lett. **106**, 153501 (2015).

[74]D. Karnaushenko, D. Makarov, C. L. Yan, R. Streubel, and O. G. Schmidt, Adv. Mater. **24**, 4518 (2012).

[75]D. Makarov, D. Karnaushenko, and O. G. Schmidt, ChemPhysChem **14**, 1771 (2013).

[76]D. Karnaushenko, D. Makarov, M. Stöber, D. D. Karnaushenko, S. Baunack, and O. G. Schmidt, Adv. Mater. **27**, 880 (2015).

[77]M. Melzer, G. G. Lin, D. Makarov, and O. G. Schmidt, Adv. Mater. **24**, 6468 (2012).

[78]M. Melzer, D. Karnaushenko, G. G. Lin, S. Baunack, D. Makarov, and O. G. Schmidt, Adv. Mater. **27**, 1333 (2015).

[79]M. Melzer, M. Kaltenbrunner, D. Makarov, D. D. Karnaushenko, D. Karnaushenko, T. Sekitani, T. Someya, and O. G. Schmidt, Nat. Commun. **6**, 6080 (2015).

[80]I. Mönch, D. Makarov, R. Koseva, L. Baraban, D. Karnaushenko, C. Kaiser, K. F. Arndt, and O. G. Schmidt, ACS Nano **5**, 7436 (2011).

[81]N. Pamme, Lab Chip **6**, 24 (2006).

[82]J. Loureiro *et al.*, Appl. Phys. Lett. **95**, 034104 (2009).

[83]J. J. Liang, L. Li, X. F. Niu, Z. B. Yu, and Q. B. Pei, Nat. Photonics **7**, 817 (2013).

[84]J. Lenz and A. S. Edelstein, IEEE Sens. J. **6**, 631 (2006).

[85]E. H. Hall, Am. J. Math. **2**, 287 (1879).

[86]W. Thomson, Proc. R. Soc. London **8**, 546 (1856).

[87]S. Yuasa, T. Nagahama, A. Fukushima, Y. Suzuki, and K. Ando, Nat. Mater. **3**, 868 (2004).

[88]L. V. Panina, K. Mohri, K. Bushida, and M. Noda, J. Appl. Phys. **76**, 6198 (1994).

[89]Y. Nishibe, H. Yamadera, N. Ohta, K. Tsukada, and Y. Nonomura, Sens. Actuator A-Phys. **82**, 155 (2000).

[90]B. Dufay, S. Saez, C. Dolabdjian, A. Yelon, and D. Menard, IEEE Trans. Magn. **49**, 85 (2013).

[91]M. Vazquez, H. Chiriac, A. Zhukov, L. Panina, and T. Uchiyama, Phys. Status Solidi A **208**, 493 (2011).

[92]P. Ripka, Sens. Actuator A-Phys. **33**, 129 (1992).

[93]D. Ernst, M. Melzer, D. Makarov, F. Bahr, W. Hofmann, O. G. Schmidt, and T. Zerna, in *37th International Spring Seminar on Electronics Technology* (IEEE, Dresden, 2014), p. 125.

[94]I. Mönch, F. Bahr, M. Melzer, D. Karnaushenko, D. Makarov, W. Hofmann, and O. G. Schmidt, IEEE Trans. Magn. **51**, 4004004 (2015).

[95]R. Koseva, I. Mönch, J. Schumann, K. F. Arndt, and O. G. Schmidt, Thin Solid Films **518**, 4847 (2010).

[96]A. Sandhu, H. Masuda, K. Kurosawa, A. Oral, and S. J. Bending, Electron. Lett. **37**, 1335 (2001).

[97]H. Bleuler, D. Vicher, G. Schweitzer, A. Traxler, and D. Zlatnik, Automatica **30**, 871 (1994).

[98]S. S. P. Parkin, Annu. Rev. Mater. Sci. **25**, 357 (1995).

[99]K. Nagasaka, J. Magn. Magn. Mater. **321**, 508 (2009).

[100]D. J. Kubinski and H. Holloway, J. Appl. Phys. **79**, 7395 (1996).

[101]M. Melzer, D. Karnaushenko, D. Makarov, L. Baraban, A. Calvimontes, I. Mönch, R. Kaltofen, Y. F. Mei, and O. G. Schmidt, RSC Adv. **2**, 2284 (2012).

[102]S. S. P. Parkin, Appl. Phys. Lett. **69**, 3092 (1996).

[103]L. Baril, B. Gurney, D. Wilhoit, and V. Speriosu, J. Appl. Phys. **85**, 5139 (1999).

[104]T. Duenas, A. Sehrbrock, M. Lohndorf, A. Ludwig, J. Wecker, P. Grunberg, and E. Quandt, J. Magn. Magn. Mater. **242**, 1132 (2002).

[105]M. Lohndorf, T. Duenas, M. Tewes, E. Quandt, M. Ruhrig, and J. Wecker, Appl. Phys. Lett. **81**, 313 (2002).

[106]T. Uhrmann, L. Bar, T. Dimopoulos, N. Wiese, M. Ruhrig, and A. Lechner, J. Magn. Magn. Mater. **307**, 209 (2006).

[107]B. Ozkaya, S. R. Saranu, S. Mohanan, and U. Herr, Phys. Status Solidi **205**, 1876 (2008).

[108]A. Bedoya-Pinto, M. Donolato, M. Gobbi, L. E. Hueso, and P. Vavassori, Appl. Phys. Lett. **104**, 062412 (2014).

[109]D. Karnaushenko *et al.*, Adv. Healthcare Mater. **4**, 1517 (2015).

[110]M. Malatek and L. Kraus, Sens. Actuator A-Phys. **164**, 41 (2010).

[111]F. L. A. Machado and S. M. Rezende, J. Appl. Phys. **79**, 6558 (1996).

[112]L. A. Tuan, N. T. Huy, and P. T. Huy, J. Phys.: Conf. Ser. **187**, 012044 (2009).

[113]K. Mohri, T. Uchiyama, L. P. Shen, C. M. Cai, L. V. Panina, Y. Honkura, and M. Yamamoto, IEEE Trans. Magn. **38**, 3063 (2002).

[114]T. Uchiyama, K. Mohri, and S. Nakayama, IEEE Trans. Magn. **47**, 3070 (2011).

[115]A. Chaturvedi, N. Laurita, A. Leary, M. H. Phan, M. E. McHenry, and H. Srikanth, J. Appl. Phys. **109**, 07B508 (2011).

[116]M. H. Phan and H. X. Peng, Prog. Mater. Sci. **53**, 323 (2008).

[117]T. Morikawa, Y. Nishibe, H. Yamadera, Y. Nonomura, M. Takeuchi, J. Sakata, and Y. Taga, IEEE Trans. Magn. **32**, 4965 (1996).

[118]T. Morikawa, Y. Nishibe, H. Yamadera, Y. Nonomura, M. Takeuchi, and Y. Taga, IEEE Trans. Magn. **33**, 4367 (1997).

[119]N. Fry, D. P. Makhnovskiy, L. V. Panina, S. I. Sandacci, D. J. Mapps, and M. Akhter, IEEE Trans. Magn. **40**, 3358 (2004).

[120]D. de Cos, N. Fry, I. Orue, L. V. Panina, A. Garcia-Arribas, and J. M. Barandiaran, Sens. Actuator A-Phys. **129**, 256 (2006).

[121]H. Jin *et al.*, Sci. Rep. **3**, 2140 (2013).

[122]B. D. Li, A. M. Morsy, and J. Kosel, IEEE Trans. Magn. **48**, 4324 (2012).

[123]N. Wacker, H. Richter, M. U. Hassan, H. Rempp, and J. N. Burghartz, Solid-State Electron. **57**, 52 (2011).

[124]S. P. Lacour, S. Wagner, R. J. Narayan, T. Li, and Z. G. Suo, J. Appl. Phys. **100**, 014913 (2006).

[125]D. H. Kim, Y. S. Kim, J. Wu, Z. J. Liu, J. Z. Song, H. S. Kim, Y. G. Y. Huang, K. C. Hwang, and J. A. Rogers, Adv. Mater. **21**, 3703 (2009).

[126]A. Carlson, A. M. Bowen, Y. G. Huang, R. G. Nuzzo, and J. A. Rogers, Adv. Mater. **24**, 5284 (2012).

[127]S. Xu *et al.*, Science **344**, 70 (2014).

[128]D. H. Kim *et al.*, Proc. Natl. Acad. Sci. U. S. A. **105**, 18675 (2008).

[129]I. Jung, G. Shin, V. Malyarchuk, J. S. Ha, and J. A. Rogers, Appl. Phys. Lett. **96**, 021110 (2010).

[130]D. H. Kim *et al.*, Appl. Phys. Lett. **93**, 044102 (2008).

[131]T. H. Han, Y. Lee, M. R. Choi, S. H. Woo, S. H. Bae, B. H. Hong, J. H. Ahn, and T. W. Lee, Nat. Photonics **6**, 105 (2012).

[132]K. Fukuda, Y. Takeda, M. Mizukami, D. Kumaki, and S. Tokito, Sci. Rep. **4**, 3947 (2014).

[133]C. Zysset, N. Münzenrieder, L. Petti, L. Buthe, G. A. Salvatore, and G. Tröster, IEEE Electron Device Lett. **34**, 1394 (2013).

[134]H. Sirringhaus, N. Tessler, and R. H. Friend, Science **280**, 1741 (1998).

[135]H. Uoyama, K. Goushi, K. Shizu, H. Nomura, and C. Adachi, Nature **492**, 234 (2012).

[136]B. Crone, A. Dodabalapur, A. Gelperin, L. Torsi, H. E. Katz, A. J. Lovinger, and Z. Bao, Appl. Phys. Lett. **78**, 2229 (2001).

[137]T. Someya, T. Sekitani, S. Iba, Y. Kato, H. Kawaguchi, and T. Sakurai, Proc. Natl. Acad. Sci. U. S. A. **101**, 9966 (2004).

[138]F. Liao, C. Chen, and V. Subramanian, Sens. Actuator B-Chem. **107**, 849 (2005).

[139]A. Sandstrom, H. F. Dam, F. C. Krebs, and L. Edman, Nat. Commun. **3**, 1002 (2012).

[140]H. Kang, H. Park, Y. Park, M. Jung, B. C. Kim, G. Wallace, and G. Cho, Sci. Rep. **4**, 5387 (2014).

[141]W. Clemens, I. Fix, J. Ficker, A. Knobloch, and A. Ullmann, J. Mater. Res. **19**, 1963 (2004).

[142]A. Yella *et al.*, Science **334**, 629 (2011).

[143]H. Zeng, C. T. Black, R. L. Sandstrom, P. M. Rice, C. B. Murray, and S. H. Sun, Phys. Rev. B **73**, 020402 (2006).

[144]R. P. Tan, J. Carrey, C. Desvaux, J. Grisolia, P. Renaud, B. Chaudret, and M. Respaud, Phys. Rev. Lett. **99**, 176805 (2007).

[145]C. T. Black, C. B. Murray, R. L. Sandstrom, and S. H. Sun, Science **290**, 1131 (2000).

[146]R. P. Tan, J. Carrey, M. Respaud, C. Desvaux, P. Renaud, and B. Chaudret, J. Magn. Magn. Mater. **320**, L55 (2008).

[147]J. Dugay *et al.*, Nano Lett. **11**, 5128 (2011).

[148]A. Weddemann *et al.*, Beilstein J. Nanotechnol. **1**, 75 (2010).

[149]J. Meyer, T. Rempel, M. Schäfers, F. Wittbracht, C. Müller, A. V. Patel, and A. Hütten, Smart Mater. Struct. **22**, 025032 (2013).

[150]H. Yan, Z. H. Chen, Y. Zheng, C. Newman, J. R. Quinn, F. Dotz, M. Kastler, and A. Facchetti, Nature **457**, 679 (2009).

[151]G. Maiellaro, E. Ragonese, A. Castorina, S. Jacob, M. Benwadih, R. Coppard, E. Cantatore, and G. Palmisano, IEEE Trans. Circuits Syst. I-Regul. Pap. **60**, 3117 (2013).

[152]Y. M. Sun, G. C. Welch, W. L. Leong, C. J. Takacs, G. C. Bazan, and A. J. Heeger, Nat. Mater. **11**, 44 (2012).

[153]C. A. Ross, Annu. Rev. Mater. Sci. **24**, 159 (1994).

[154]O. Graudejus, P. Gorrn, and S. Wagner, ACS Appl. Mater. Interfaces **2**, 1927 (2010).

[155]E. Cerda, K. Ravi-Chandar, and L. Mahadevan, Nature **419**, 579 (2002).

[156]S. P. Lacour, S. Wagner, Z. Y. Huang, and Z. Suo, Appl. Phys. Lett. **82**, 2404 (2003).

[157]S. P. Lacour, D. Chan, S. Wagner, T. Li, and Z. G. Suo, Appl. Phys. Lett. **88**, 204103 (2006).

[158]S. S. P. Parkin, Z. G. Li, and D. J. Smith, Appl. Phys. Lett. **58**, 2710 (1991).

[159]N. Bowden, S. Brittain, A. G. Evans, J. W. Hutchinson, and G. M. Whitesides, Nature **393**, 146 (1998).

[160]E. Cerda and L. Mahadevan, Phys. Rev. Lett. **90**, 074302 (2003).

[161]J. Genzer and J. Groenewold, Soft Matter **2**, 310 (2006).

[162]Z. Y. Huang, W. Hong, and Z. Suo, J. Mech. Phys. Solids **53**, 2101 (2005).

[163]D. Y. Khang, H. Q. Jiang, Y. Huang, and J. A. Rogers, Science **311**, 208 (2006).

[164]W. M. Choi, J. Z. Song, D. Y. Khang, H. Q. Jiang, Y. Y. Huang, and J. A. Rogers, Nano Lett. **7**, 1655 (2007).

[165]N. Bowden, W. T. S. Huck, K. E. Paul, and G. M. Whitesides, Appl. Phys. Lett. **75**, 2557 (1999).

[166]P. Cendula, S. Kiravittaya, I. Mönch, J. Schumann, and O. G. Schmidt, Nano Lett. **11**, 236 (2011).

[167]F. Brau, H. Vandeparre, A. Sabbah, C. Poulard, A. Boudaoud, and P. Damman, Nat. Phys. **7**, 56 (2011).

[168]P. G. Sanders, J. A. Eastman, and J. R. Weertman, Acta Mater. **45**, 4019 (1997).

[169]H. Doi, Y. Fujiwara, K. Miyake, and Y. Ossawa, Metallurgical and Materials Transactions B **1**, 1417 (1970).

[170]S. X. Wang and G. Li, IEEE Trans. Magn. **44**, 1687 (2008).

[171]A. Hütten *et al.*, J. Biotechnol. **112**, 47 (2004).

[172]A. Fornara *et al.*, Nano Lett. **8**, 3423 (2008).

[173]O. V. Salata, J. Nanobiotechnol. **2**, 3 (2004).

[174]I. Mönch, A. Meye, A. Leonhardt, K. Krämer, R. Kozhuharova, T. Gemming, M. P. Wirth, and B. Büchner, J. Magn. Magn. Mater. **290**, 276 (2005).

[175]D. R. Baselt, G. U. Lee, M. Natesan, S. W. Metzger, P. E. Sheehan, and R. J. Colton, Biosens. Bioelectron. **13**, 731 (1998).

[176]S. L. Chiu, J. Leu, and P. S. Ho, J. Appl. Phys. **76**, 5136 (1994).

[177]H. B. Huang and F. Spaepen, Acta Mater. **48**, 3261 (2000).

[178]T. Sakai, H. Miyagawa, G. Oomi, K. Saito, K. Takanashi, and H. Fujimori, J. Phys. Soc. Jpn. **67**, 3349 (1998).

[179]M. Melzer, A. Kopylov, D. Makarov, and O. G. Schmidt, SPIN **3**, 1340005 (2013).

[180]D. A. Hall, R. S. Gaster, T. Lin, S. J. Osterfeld, S. Han, B. Murmann, and S. X. Wang, Biosens. Bioelectron. **25**, 2051 (2010).

[181]A. Weddemann *et al.*, Biosens. Bioelectron. **26**, 1152 (2010).

[182]P. Tseng, J. Lin, K. Owsley, J. Kong, A. Kunze, C. Murray, and D. DiCarlo, Adv. Mater. **27**, 1083 (2015).

[183]R. Blakemore, Science **190**, 377 (1975).

[184]W. Wiltschko and R. Wiltschko, J. Comput. Physiol. A **191**, 675 (2005).

[185]M. Ying, A. P. Bonifas, N. S. Lu, Y. W. Su, R. Li, H. Y. Cheng, A. Ameen, Y. G. Huang, and J. A. Rogers, Nanotechnology **23**, 344004 (2012).

[186]Y. W. Su, R. Li, H. Y. Cheng, M. Ying, A. P. Bonifas, K. C. Hwang, J. A. Rogers, and Y. G. Huang, J. Appl. Phys. **114**, 164511 (2013).

[187]S. W. Kwok *et al.*, Adv. Funct. Mater. **24**, 2180 (2014).

[188]Z. Suo, E. Y. Ma, H. Gleskova, and S. Wagner, Appl. Phys. Lett. **74**, 1177 (1999).

[189]S. D. Bader and S. S. P. Parkin, *Annual Review of Condensed Matter Physics* (Annual Reviews, Palo Alto, 2010), Vol. 1, p. 71.

[190]J. M. Hu, Z. Li, L. Q. Chen, and C. W. Nan, Nat. Commun. **2**, 553 (2011).

[191]D. A. Allwood, G. Xiong, C. C. Faulkner, D. Atkinson, D. Petit, and R. P. Cowburn, Science **309**, 1688 (2005).

[192]D. Karnaushenko, N. Münzenrieder, D. D. Karnaushenko, B. Koch, A. K. Meyer, S. Baunack, L. Petti, G. Tröster, D. Makarov, and O. G. Schmidt, Adv. Mater. **27**, 6797 (2015).

[193]D. Karnaushenko, D. D. Karnaushenko, D. Makarov, S. Baunack, R. Schäfer, and O. G. Schmidt, Adv. Mater. **27**, 6582 (2015).